Report of the National Research Institute for Earth Science and Disaster Prevention, No, 57 ; December, 1996

A Numerical Simulation of Strong Ground Motions of Rather Long Periods near Earthquake Faults Including Effects of Deep Soil Deposits

By

Fumio YAMAMIZU*

National Research Institute for Earth Science and Disastar Prevention (NIED), 3-1 Tennodai, Tsukuba, Ibaraki, 305 Japan

Abstract

Assuming a large earthquake like the Kanto Earthquake of 1923, ground motions in the epicentral area were theoretically synthesized by introducing the effect of inhomogeneous rupture propagation and taking the thick sedimentary layers into consideration. The ground motions synthesized for the seven sites in and around the Tokyo metropolitan area, Tokyo, Yokohama, Hatano, Fuchu, Chiba, Kamogawa, and Tateyama, clearly demonstrate the drastic effect of the thick sedimentary layers in comparisons with the results for the half space model. From an engineering point of view, influences of the synthesized motions upon artificial structures were evaluated in terms of the response spectra. The response spectra show that the structures with rather long fundamental periods are severely affected by the ground motions. For the period range longer than 3 seconds, the response spectra surpass the upper limit of the Architectural Institutes of Japan (AIJ) recommendation on the base shear at all the sites where the ground motions were synthesized.

Keywords : Strong Ground Motion, Near Field, Inhomogeneous Source, Deep Soil Deposit, Simulation, Kanto Earthquake

1. Introduction

For designing anti-seismic structures, it is indispensable to clarify the characteristics of strong ground motions in the epicentral area of major earthquakes. The earthquake motions integratedly include the source kinematics, path effects, and local site conditions, so that it is natural that the earthquake motions are treated as a whole including all those effects. Most of the past studies in earthquake engineering, however, stressed only the local site effect near the structure, because their interests were mainly directed at short period ground motions, such as those less than 1 second. For short period waves, it is very difficult to apply such total treatment, since the source kinematics and wave propagation are quite complex. By taking all effects described above into consideration, Ohta and Kagami (1976) and Kudo (1978) proposed an idea for treating the body and surface wave propagation from source to structures for those seismic waves with a fairly long period. Their proposals are simple and adaptable for estimating the behavior of large scale structures which have a rather long fundamental period of 5-10 seconds.

On the other hand, recent studies in seismology advanced various mathematical techniques for simulating ground motions by introducing more realistic source kinematics and medium structures. In the beginning, these were only applied to unbounded homogeneous mediums (e.g., Aki, 1968 ; Kanamori, 1972). Then, the free surface effect (e.g., Kawasaki *et al.*, 1973, 1975 ; Bouchon and Aki, 1977), and the effect of sedimentary layers (e.g., Heaton and Helmberger, 1977, 1978 ; Bouchon, 1979a, b) were gradually included in the simulation. The development of modeling the

*Advanced Measurement and Analysis Technology Division, Computational Sciences Laboratory.

earthquake source process revealed a nonuniform rupturing process (e.g., Miyatake, 1980a, b ; Aki, 1982). Hybrid models were proposed for predicting the high-frequency acceleration, in which gross features of the rupture process are specified deterministically, but details of the process are described by a stochastic model specified by a small number of parameters (Aki, 1982). By using those mathematical techniques, the total treatment of the strong ground motion seems to have become possible not only for long period waves but also for short period ones. But yet, the applicablity for the shorter waves still seems to be difficult because those waves are seriously affected by the diversity of local site conditions.

In the present paper, we synthesized strong ground motions expected in the epicentral area of a major earthquake. Although our interests were restricted to the rather long period range, the synthesized motions included whole effects of source and propagation. For the seismic source, the Kanto Earthquake of 1923 was modeled by introducing inhomogeneous rupture propagation in order to generate rather short period waves. The layered underground structure was set up by taking realistic thick sedimentary layers into account. From an engineering point of view, influences of the synthesized motions upon large-scale structures were simply evaluated in terms of the response spectra.

2. Synthesizing Technique

The ground motions by an earthquake are generally computed by a space-time convolution of slip function with Green function (Aki and Richards, 1980 ; Aki, 1982). The slip function describes the fault displacement during an earthquake as a function of time and position on the fault plane. The Green function represents the impulse response of a medium to a force system applied at a point on the fault plane. The slip function and the Green function represent the source and the propagation effect on seismic motion, respectively. The source effect, even though it is very complex in space and time, can be modeled by giving a distribution of point sources on the fault plane, then the total wave field is represented by a superposition of the Green functions for each point source. Therefore, the computation of the Green function for a realistic medium is essential to obtain reliable results.

There are many approaches for evaluating the Green function ; generalized ray theory (Helmberger, 1974 ; Helmberger and Harkrider, 1978), reflectivity method (Fucks, 1968 ; Fucks and Muller, 1971), reflection and transmission matrix method (Aspel, 1979 ; Kennett and Kerry, 1979 ; Kennett, 1980 ; Luco and Aspel 1983 ; Aspel and Luco, 1983), discrete wavenumber method (Bouchon, 1981), and extended reflectivity method (Kohketsu, 1985). Among those methods, Yao and Harkrider's (1983) technique was employed in this study. This approach is based on Kennett and Kerry's (1979) generalized reflection and transmission matrix method for the wavenumber integrands and Bouchon's (1981) discrete wavenumber method for the wavenumber integration.

For the point shear dislocation in a layered medium, integral solutions of the surface radial, tangential, and vertical displacements in the frequency domain are

$$
\begin{aligned}
u(\omega) &= \frac{iM(\omega)}{4\pi\rho\omega^2}\sum_{m=0}^{2} C_m \int_0^\infty \left[iU_m(k,\omega)\frac{dJ_m(kr)}{d(kr)} - V_m(k,\omega)\frac{J_m(kr)}{kr} \right] kdk \\
v(\omega) &= \frac{iM(\omega)}{4\pi\rho\omega^2}\sum_{m=1}^{2} C'_m \int_0^\infty \left[iU_m(k,\omega)\frac{mJ_m(kr)}{kr} - V_m(k,\omega)\frac{dJ_m(kr)}{d(kr)} \right] kdk \\
w(\omega) &= \frac{iM(\omega)}{4\pi\rho\omega^2}\sum_{m=0}^{2} C_m \int_0^\infty W_m(k,\omega) J_m(kr) kdk
\end{aligned}
\tag{1}
$$

respectively, where ρ is medium density, $M(\omega)$ is seismic moment (source function), and C_m and C'_m represent the radiation pattern. The radiation pattern coefficients are related to the fault geometry, and their explicit expressions are

$$
\begin{aligned}
&C_0 = a_2, \\
&C_1 = a_1\cos\varphi - b_1\sin\varphi, \quad C_1' = -a_1\sin\varphi - b_1\cos\varphi, \\
&C_2 = a_2\cos 2\varphi - b_2\sin 2\varphi, \quad C_2' = -a_2\sin 2\varphi - b_2\cos 2\varphi, \\
&\quad a_1 = \cos\delta\cos\lambda, \quad b_1 = \cos 2\delta\sin\lambda, \\
&\quad a_2 = \frac{1}{2}\sin 2\delta\sin\lambda, \quad b_2 = -\sin\delta\cos\lambda,
\end{aligned}
$$

where φ is the azimuth to the receiver relative to the fault strike, δ is the dip angle of the fault, and λ is the rake angle of slip on the fault. The wavenumber integrations involved in the above solutions (1) have a form of

$$
I_m = \int_0^\infty F(k,\omega) J_m(kr) kdk.
$$

According to Bouchon (1981), this type of integration is efficiently evaluated by replacing the wavenumber integral by the discrete wavenumber summation as

$$
I_m = \frac{\pi}{L}\sum_{j=0}^{\infty} e_j k_j F(k_j,\omega) J_m(k_j r)
$$

$$e_j=\begin{cases} 2 & for \quad j\neq 0 \\ 1 & for \quad j=0 \end{cases} \qquad k_j=\frac{2\pi j}{L}$$

if epicentral distance r, source depth d, and discretization distance L satisfied $r<L/2$ and $\sqrt{(L-r)^2+d^2}>\alpha t$, where α and t are the P wave velocity and the time interval concerned, respectively.

The kernels U_m and W_m in the integral equation (1) are the displacement generated by the P and SV wave source potentials, while V_m is by the SH potential. These kernels depend on wavenumber, frequency, source depth, and layer parameters, and are evaluated by using the generalized reflection and transmission matrices given by Kennett and Kerry (1979). By using the same notation, the solutions on the free surface are represented by

$$\begin{bmatrix} U_m \\ W_m \end{bmatrix}=(\mathbf{M}_U+\mathbf{M}_D\mathbf{R})(\mathbf{I}-\mathbf{R}_D^{RS})^{-1}$$
$$\mathbf{T}_U^{RS}(\mathbf{I}-\mathbf{R}_D^{SL}\mathbf{R}_U^{FS})^{-1}\left(\mathbf{R}_D^{SL}\begin{bmatrix} P_m^+ \\ S_m^+ \end{bmatrix}+\begin{bmatrix} P_m^- \\ S_m^- \end{bmatrix}\right)$$

for P-SV waves, and

$$V_m=2k(1-R_D^{RS})^{-1}T_U^{RS}(1-R_D^{SL}R_U^{FS})^{-1}(R_D^{SL}H_m^{+}+H_m^{-})$$

for SH wave. The terms $P_m^{\pm}$, $S_m^{\pm}$, and $H_m^{\pm}$ represent the P, SV, and SH wave source potential, and the plus or minus superscripts correspond to the downward or upward propagating waves, respectively. The source terms are

$$P_0^{\pm}=-\frac{3k^2-2k_\alpha^2}{\nu_\alpha}, \quad S_0^{\pm}=-3ik[s], \quad H_0^{\pm}=0,$$
$$P_1^{\pm}=2ik[s], \quad S_1^{\pm}=\frac{2k^2-k_\beta^2}{\nu_\beta}, \quad H_1^{\pm}=-\frac{ik_\beta^2[s]}{k},$$
$$P_2^{\pm}=-\frac{k^2}{\nu_\alpha}, \quad S_2^{\pm}=ik[s], \quad H_2^{\pm}=\frac{k_\beta^2}{\nu_\beta},$$

where

$$k_\alpha=\frac{\omega}{\alpha}, \quad k_\beta=\frac{\omega}{\beta},$$
$$\nu_\alpha^2=k_\alpha^2-k^2, \quad \nu_\beta^2=k_\beta^2-k^2, \quad \mathrm{Im}(\nu_{\alpha,\beta})<0$$
α = P wave velocity, β = S wave velocity,

and $[s]=\pm 1$ for the plus or minus superscript.

3. Structure Model, Fault Model, and Numerical Examples

3.1 Structure Model with Sedimentary Layers

In the Tokyo metropolitan area, thick soils are widely deposited to the depth of several kilometers. According to the computations by Yamamizu and Goto (1978), Ohta *et al.* (1980), and Yamamizu *et al.* (1983) about the amplification of SH wave by the thick sedimentary layers, it is certain that rather long period seismic motions are severely affected by those thick sedimentary layers. Therefore, the effect of thick sedimentary layers are very important for estimating realistic ground motions of rather long periods.

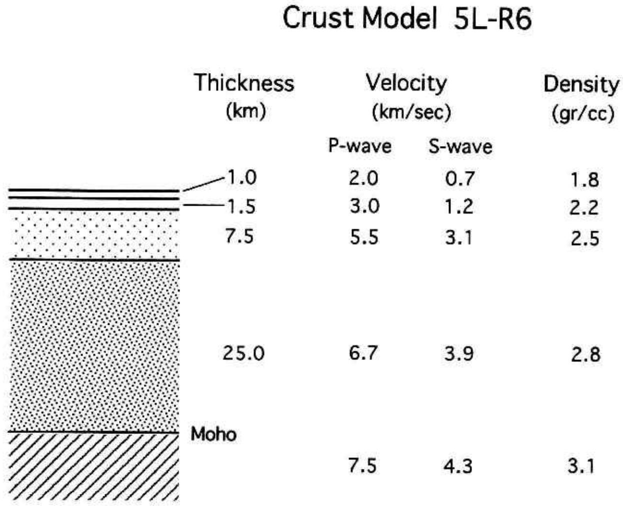

Fig. 1 Simplified layered structure model, 5L-R6, used for waveform synthesis.

The layered structure model, 5L-R6, adopted in the present simulation is shown in Fig. 1. The upper two are sedimentary layers, which were modeled on the basis of the results of down-hole measurements carried out at three deep holes in Iwatsuki, Shimohsa, and Fuchu (double circles in Fig. 2) in the Tokyo metropolitan area (Ohta *et al.*, 1977, 1978 ; Yamamizu *et al.* 1981, 1983) and the results of refraction prospecting from the Yumenoshima explosions (Shima *et al.*, 1976a, b ; Seo and Kobayashi, 1980). Roughly speaking, the uppermost layer is composed of Narita and Kazusa groups of Pleistocene soils, and the second one of Miura and other groups of Miocene. The P and S wave velocities of those layers are 2.0 and 0.7km/sec for the first layer and 3.0 and 1.2 km/sec for the second one, respectively. For densities, we used the gamma-ray logging data also obtained in the three deep holes at Iwatsuki, Shimohsa, and Fuchu (Suzuki *et al.* 1981 ; Takahashi, 1982). For the lower structure under the sediment, we followed the result by Seo (1979), which gives a representative crust-mantle structure in the southern Kanto district. The depth to the lowest interface is 35km, corresponding to the Moho discontinuity. The attenua tion factor, Q, was not included in order to simplify the computation because the effect may not be serious for the rather long period band considered (Yamamizu *et al.*, 1983 ; Takeo, 1985).

3.2 Inhomogeneous Fault Model as a Superposition of Point Sources

In Fig. 2, the fault plane assumed and locations for waveform synthesis are shown by a square and large solid circles, respectively. The fault geometry is nearly the same as that for the 1923 Kanto earthquake estimated by Kanamori (1974). Details are summarized in Table 1, in comparison with Kanamori's Model. The small solid circle on the southern side of the fault plane represents the epicenter, and rupture starts at this point. The fault plane of 120km by 70 km was divided into 20×10 subfaults with a $6 \times 7 km^2$ area, and each subfault was replaced by a double-couple point source. The strike, dip, and rake angles are common for all the point sources. But the other parameters, such as the seismic moment and rise-time, differ for each point source. In addition, the origin time of each point source is shifted one by one to represent an irregular rupture propagation.

The irregular rupture process was given *a priori* by referring to Miyatake's (1980a) result, in which the rupturing process on the fault surface with random strength distribution was numerically simulated by a three-dimensional crack propagation by using the finite difference approximation. In Fig. 3, the rupture process assumed is shown in four maps for every 10 seconds by contours of rupture front at every 2 seconds. Total rupturing time is about 35 seconds. The moment (dislocation) and rise-time distribution are shown in Fig. 4 and Fig. 5, respectively. The seismic moment is represented by the distribution of dislocation on subfaults because the area is the same for all

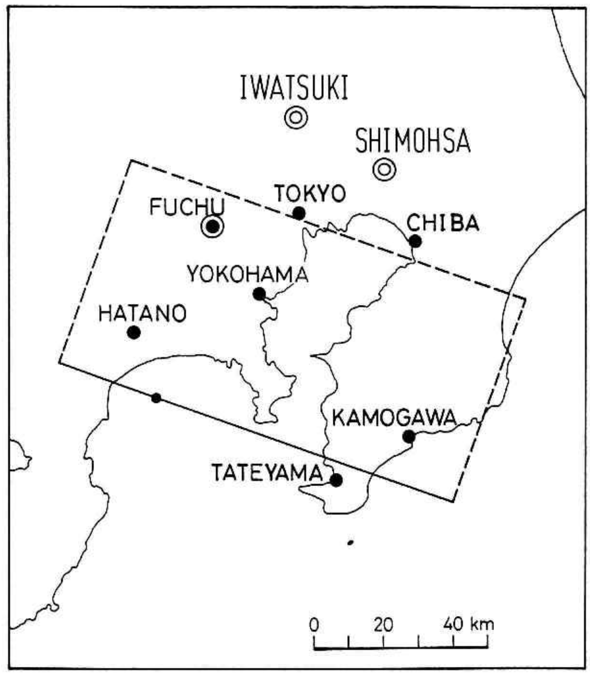

Fig. 2 Projection of the assumed fault plane upon the ground surface, and positions of Tokyo, Yokohama, Hatano, Fuchu, Chiba, Kamogawa, and Tateyama where the strong ground motions are synthesized. Double circles are the three Deep Borehole Observatories of Iwatsuki, Shimohsa, and Fuchu where downhole measurements were carried out for precise estimation of the sedimentary structure.

Table 1 Summary of the assumed geometry

		This Study	Kanamori Model
Epicenter	Longitude	139.3° E	139.3° E
	Latitude	35.2° N	35.2° N
	Depth	2.5 km	0 km
Fault	Width	70 km	70 km
	Length	120 km	130 km
	Dip Direction	N 20° E	N 20° E
	Dip Angle	28°	34°
Slip (right lateral reverse)	Rake Angle	18°	18°
Rupture	Process	Random	Bilateral
	Veloity		3.0 km/sec
	Rise Time	2-5 seconds	5.0 seconds

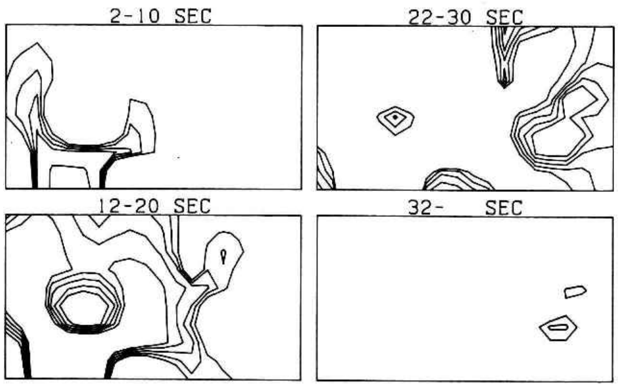

Fig. 3 Contour maps of the rupture front for every 10 seconds. In each map, contours are drawn at every 2 seconds.

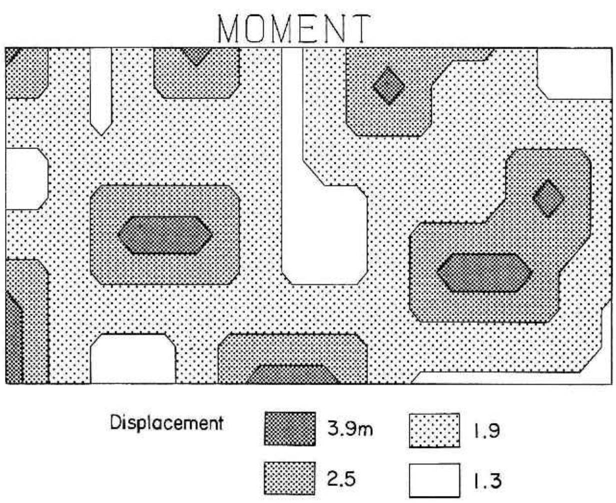

Fig. 4 Distribution of the moment (dislocation) of point sources on the main fault.

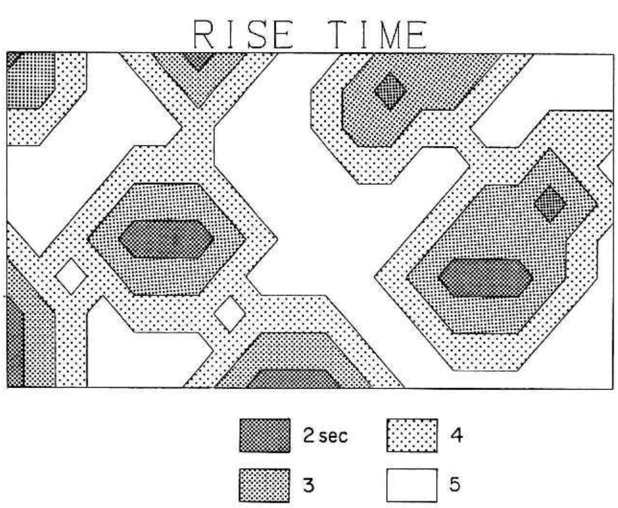

Fig. 5 Distribution of the rise-time of point sources on the main fault.

subfaults. The total moment is 5.3×10^{27} dyne-cm, and hence the average dislocation over the fault surface is estimated as about 2.1 meters.

The source time function is ordinarily represented by the ramp-type function. Among various ramp functions, we adopted a smoothly varying function ;

$$S_d(t)=\frac{1}{2}\left\{1+\tanh\left(\frac{2t}{t_r}-1\right)\right\} \tag{2}$$

where t_r is rise-time. The moment function in the integral solutions of (1) is, therefore, represented by

$$M_d(\omega)=\pi\delta(\omega)-i\frac{\pi t_r}{4}\exp(-i\frac{\omega t_r}{2})\text{cosech}\frac{\pi\omega t_r}{4}$$

in the frequency domain by the Fourier transform of $S_d(t)$ in equation (2), where $\delta(\omega)$ is Dirac's delta function. On the other hand, when the velocity-type waveform is synthesized, we must adopt a derivative of $S_d(t)$, that is,

$$S_v(t)=\frac{1}{t_r}\text{sech}^2(\frac{2t}{t_r}-1)$$

and the corresponding moment function is

$$M_v(\omega)=\frac{\pi\omega t_r}{4}\exp\left(-i\frac{\omega t_r}{2}\right)\text{cosech}\frac{\pi\omega t_r}{4}$$

The actual synthesis was done for velocity waveforms by using $M_v(\omega)$, then displacement waveforms are obtained by a numerical integration.

3.3 Numerical Examples

To check the computer program and concurrently to illustrate the influence of sedimentary layers upon the seismic motions, we made preliminary computations for two cases. The first one assumed that a point shear dislocation source is embedded in mediums of different types. The second one is for a finite fault in the half-space medium, in which the rupture propagates bilaterally.

3.3.1 Point source embedded in the layered medium

The point source, fixed at a depth of 5km, was assumed to be of the same focal mechanism as is shown in Table 1, and the rise time was chosen at 0.25 seconds. Figure 6 illustrates the resulting waveforms on the ground surface at a site which is located

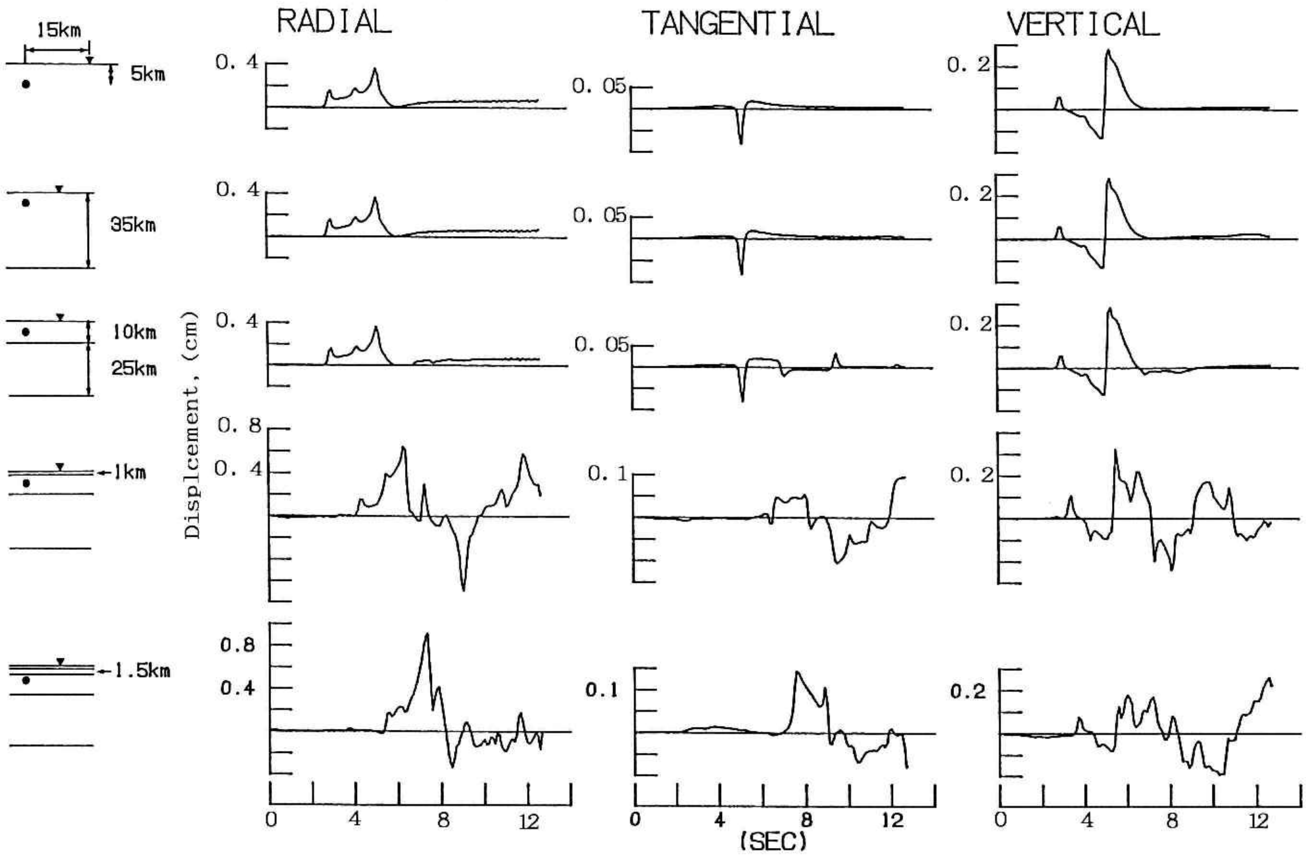

Fig. 6 Examples of the synthesized ground motions. Left-hand column shows the structure models used, in which layers are added one by one in order to check the effect of layering upon the synthesized waveform.

15km away. Azimuth of the site is 30° relative to the fault strike. In this figure, the medium was at first assumed as a half-space (top figure), then, was modified step by step to the model shown in Fig. 1 (bottom figure). The later phase, which is clearly seen especially in the tangential component of the two-layer model, is the multiple reflection within the uppermost layer. Except for this later phase, the waveforms are very similar to each other for the upper three cases. However, for the lower two cases where thin sedimentary layers are added, not only the waveform but also the amplitude are drastically changed. It is seen in those traces that rather long period motions of 4-6 seconds are excited by sedimentary layers. From this fact, we can clearly understand the striking effect of the sedimentary layers.

3.3.2 Finite fault with bilateral rupture

We model a finite fault following the Kanamori's (1974) study. Kanamori (1974) computed the ground motions at Tokyo for the finite fault in the half-space medium assuming the bilateral rupture propagation. In Figure 7, we compare the displacement waveforms by Kanamori (left) with those of the present study (right) which assumed nearly the same fault geometry and bilateral rupture (Table 1).

The features of both waveform sets are very similar to each other. By watching carefully, a small discrepancy appears around the onset of EW waveform. This discrepancy may be caused by the difference of the dip-angle (Table 1) and/or the computing method for the rupture propagation; the propagation effect is evaluated by numerical integration in Kanamori's study, while by superposition of point sources in the present one. In any case, the difference is negligibly small, so that the present superposition method is sufficient to compute the rupture propagation effect.

4. Synthesized Ground Motions

On the basis of the fault model described in the previous section 3.2, the ground motions were synthesized at seven sites in and around the Tokyo metropolitan area. The locations are shown in Fig. 2 ; Tokyo,

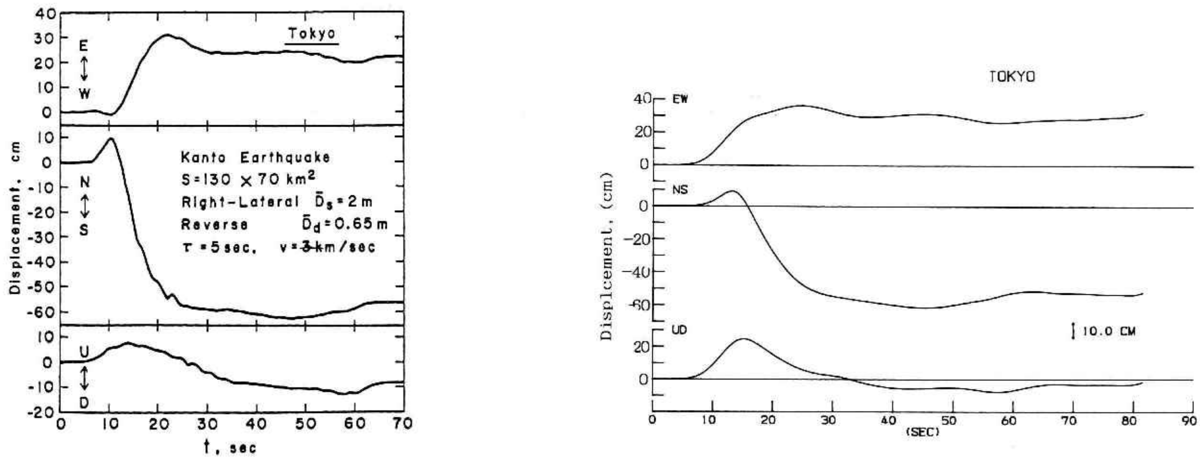

Fig. 7 Comparison of synthesized displacement waveforms of the present study (right) with those of Kanamori (1974) (left). Kanamori's coordinate system was not directed to real east and north but was rotated counterclockwise 23 degree.

Yokohama, Hatano, Fuchu, Chiba, Kamogawa, and Tateyama. The sediment structure is different from site to site, so that it is natural to use a three-dimensional underground structure for synthesizing the ground motions. Unfortunately, there is no available computer facility and effective code for computing those three-dimensional propagations within a realistic computer-time in the present stage. For this reason, we assumed the same underground structure at all the sites, and so the difference between each site depends only on the position in relation to the fault geometry. Hereafter, "the layered model" means the underground structure model of Fig. 1. Similarly, parameters of "the half-space model" are 5.5km/sec, 3.1km/sec, and 2.5gr/cm³ for P wave, S wave velocity, and density, respectively. The synthesized

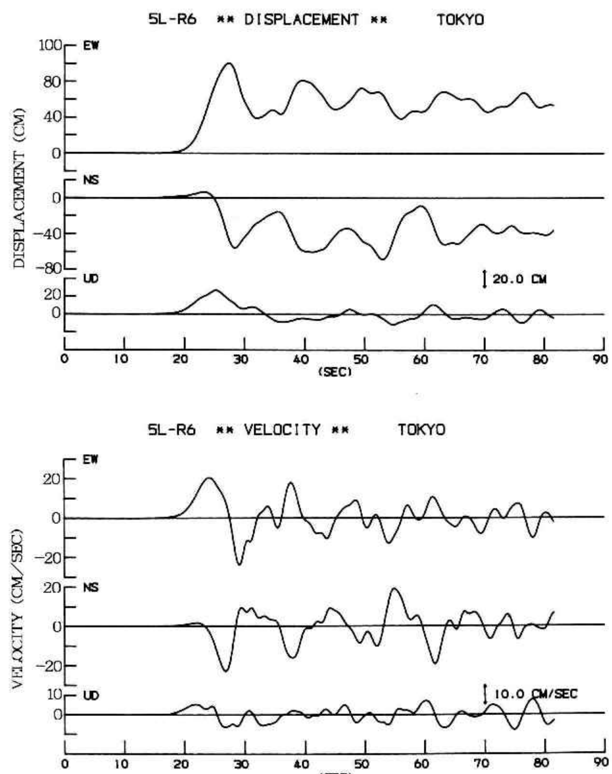

Fig. 8a Synthesized displacement (upper) and velocity (lower) waveforms at Tokyo for the layered structure model. The unit of vertical axis is shown in the figure.

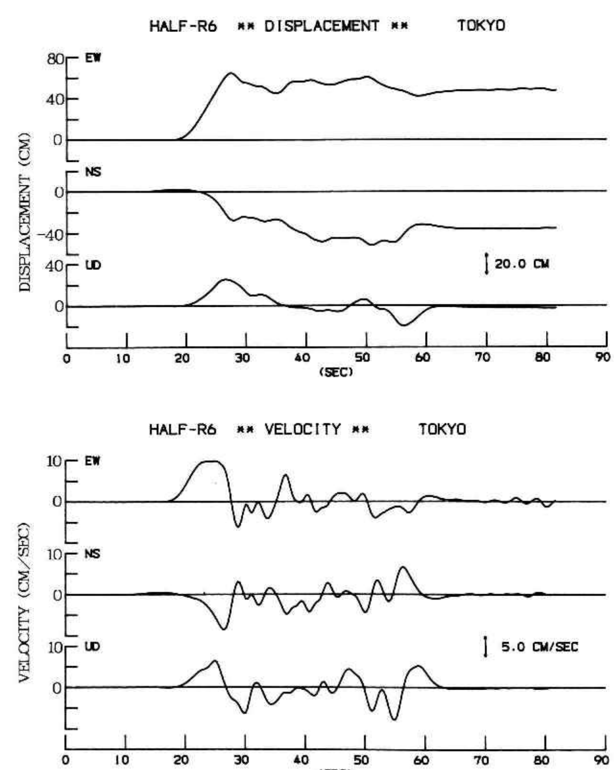

Fig. 8b Synthesized displacement (upper) and velocity (lower) waveforms at Tokyo for the half-space model. The unit of vertical axis is shown in the figure.

waveforms at the seven sites are shown in Figs. 8-14. In those figures, the origin of time-axis was set at the start-time of rupture (origin-time).

The first site we consider, Tokyo, is located to the northeast of the epicenter at a distance of about 65 km, and lies just on the lower fault edge which is dipping toward $N20°E$ (Fig. 2). The displacement and velocity waveforms at Tokyo for the layered model are shown in Fig. 8a, and those for the half-space model are presented in Fig. 8b. By comparing these two waveform sets, we can see at a glance that long period motions of 10-13 seconds are predominant in the former synthetics for the layered structure model. It is clear that the long period motions are effectively excited by the layered structure, because no such motions appear in the synthetics for the half-space model (Fig. 8b). The ground motions for the half-space model are restricted to about 40 seconds from 20 to 60 seconds on the time axis corresponding to the total time of fault rupturing. The complex motions in this time interval immediately reflect irregularities of the source process. This situation is common to all the following cases. On the other hand, a much longer duration of the ground motion is seen for the layered model (Fig. 8a).

The second site, Yokohama, is located above a middle part of the fault, and about 40km apart from the epicenter toward the northeast. The synthesized waveforms at Yokohama for the layered and the half-space models are shown in Fig. 9a and Fig. 9b, respectively. It is notable that longer period motions of 10-15 seconds are outstanding in the EW component after 50 seconds, but relatively short period waves of 2-4 seconds are predominant in the NS component for the same time interval. The displacement rises up rather slowly, taking about 15 seconds, and reaches about 100cm in EW component and 60cm in NS component. At nearly 30 seconds, a large impulsive velocity with a period of 4-6 seconds is conspicuous, and we expect a large acceleration at this instance.

Hatano is the nearest to the epicenter ; the epicentral distance is about 20km. The synthesized waveforms are shown in Fig. 10a and Fig. 10b. At this site, damages caused by the 1923 Kanto earthquake were very severe. According to Kanamori's (1974) simulation the amplitude of ground displacement was about twice as large as that in Tokyo. As expected by that fact, the synthesized waveforms at Hatano show the largest velocity among the seven sites ; about 30-

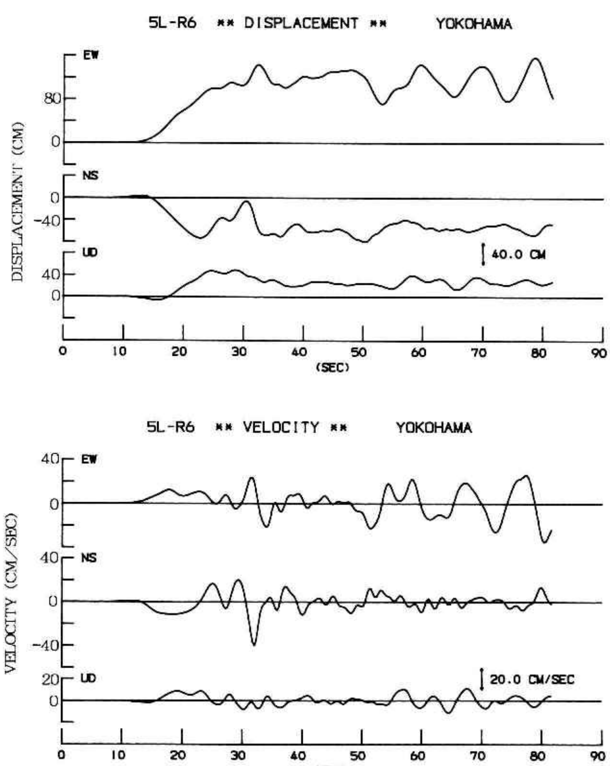

Fig. 9a Synthesized displacement (upper) and velocity (lower) waveforms at Yokohama for the layered structure model. The unit of vertical axis is shown in the figure.

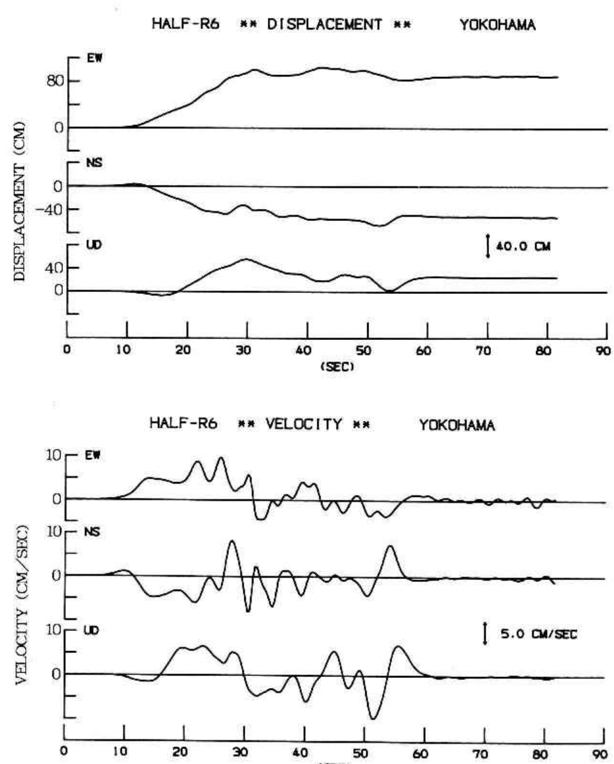

Fig. 9b Synthesized displacement (upper) and velocity (lower) waveforms at Yokohama for the half-space model. The unit of vertical axis is shown in the figure.

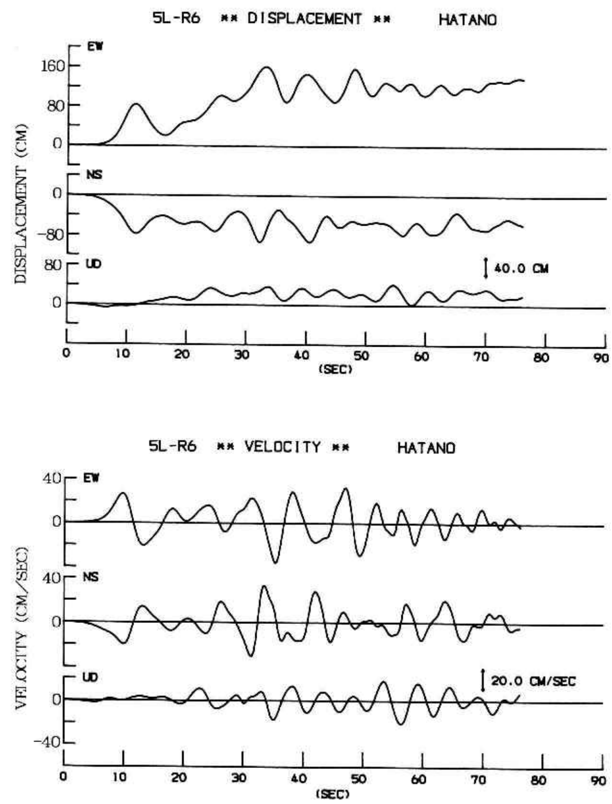

Fig. 10a Synthesized displacement (upper) and velocity (lower) waveforms at Hatano for the layered structure model. The unit of vertical axis is shown in the figure.

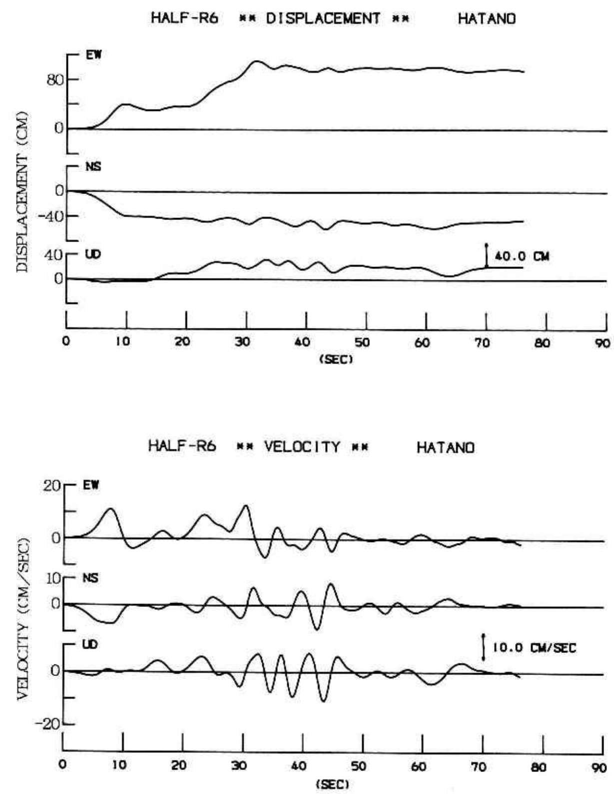

Fig. 10b Synthesized displacement (upper) and velocity (lower) waveforms at Hatano for the half-space model. The unit of vertical axis is shown in the figure.

40cm/sec in both components for the layered model as shown in Fig. 10a. Also, the displacements of 120-140cm in the EW and 40-60cm in the NS components are the largest. In addition, the synthesized motions have two characteristic features. The first one is the monotonical wavetrain lasting for a long time, which is seen in the velocity waveforms shown in Fig. 10a. By comparing Fig. 10a with Fig. 10b, we understand that the monotonical wavetrain is originally excited by the faulting process, and then remarkably amplified and prolonged by the layered structure. The period of the wavetrain is about 7 seconds. It is anticipated that the wavetrain will seriously affect the structures having a similar fundamental period. The second feature is two steplike changes in the displacement, which are clearly seen in the EW component of the half-space synthetics shown in Fig. 10b. At the first stage, the displacement is growing up to about 40cm in both the EW and NS components. But at second stage about 20 seconds after the first arrival, the motion progresses only in the EW direc tion, and the EW displacement reaches to about 90-100cm. Those steplike changes are also seen in the synthetics for the layered model (Fig. 10a). This nature of displacement may be caused by the rupturing process.

Fuchu is located in the western half area of the fault similar to Hatano, but is about 50km apart from the epicenter along the dip-direction of the fault. The synthetic waveforms at Fuchu are shown in Fig. 11a, and Fig.11b. The velocity waveforms have a common feature with Hatano in that a monotonic wavetrain appears. In this case, however, the period is as short as 3-4 seconds. Since 3-4 seconds corresponds to the fundamental period of the so-called "S structure building" (having a steel structure for the main part) of 25-35 stories (Ohtani, 1977), the predicted motions at this site may be more dangerous than those at Hatano.

Chiba and Kamogawa are located at about 80km from the epicenter, but the latter is near the fault edge like Hatano. In Figs. 12a, b, and 13a, b, the synthesized waveforms at Chiba and Kamogawa are shown, respectively. The velocity waveforms at both sites are similar to each other. At the beginning of the velocity waveform, there is a large two-cycle oscillatory motion of about a 10 seconds period. The oscillatory motion may originate from the rupturing process. The

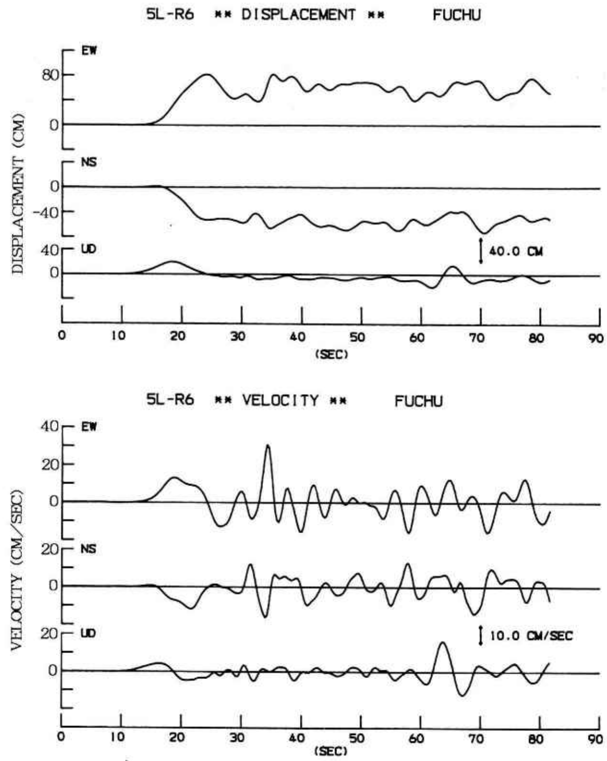

Fig. 11a Synthesized displacement (upper) and velocity (lower) waveforms at Fuchu for the layered structure model. The unit of vertical axis is shown in the figure.

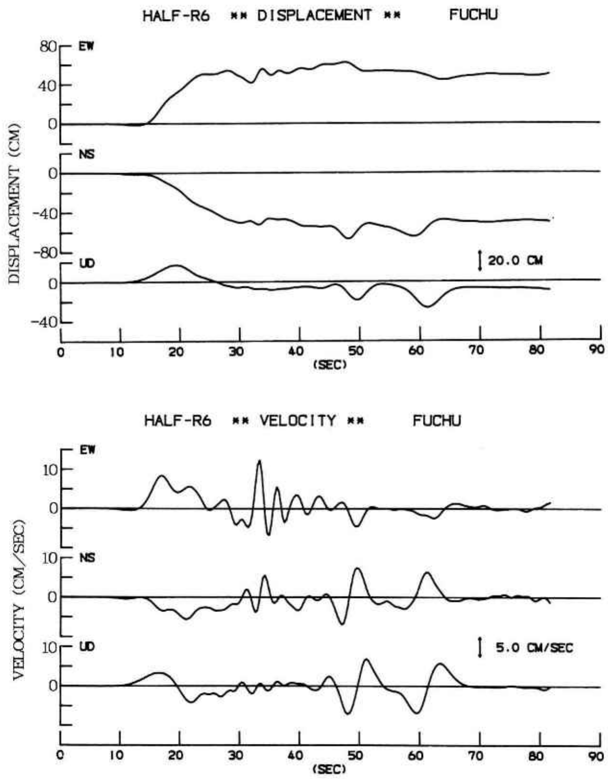

Fig. 11b Synthesized displacement (upper) and velocity (lower) waveforms at Fuchu for the half-space model. The unit of vertical axis is shown in the figure.

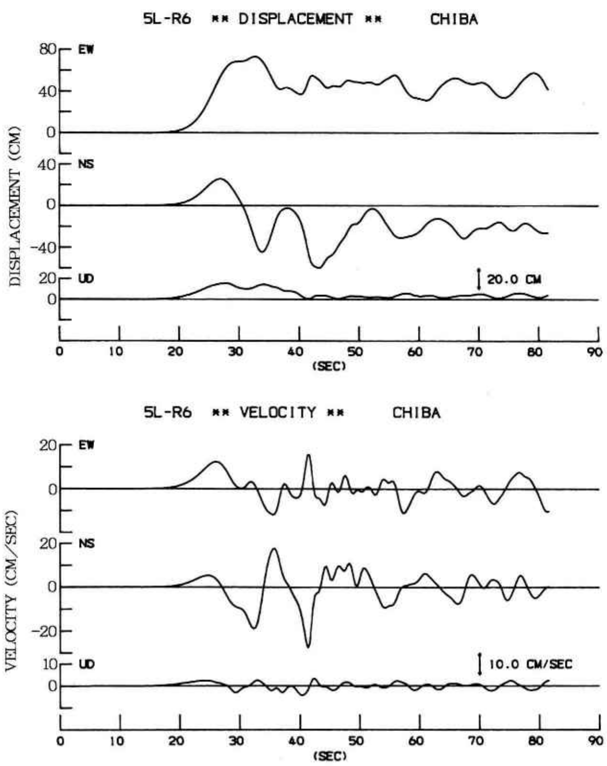

Fig. 12a Synthesized displacement (upper) and velocity (lower) waveforms at Chiba for the layered structure model. The unit of vertical axis is shown in the figure.

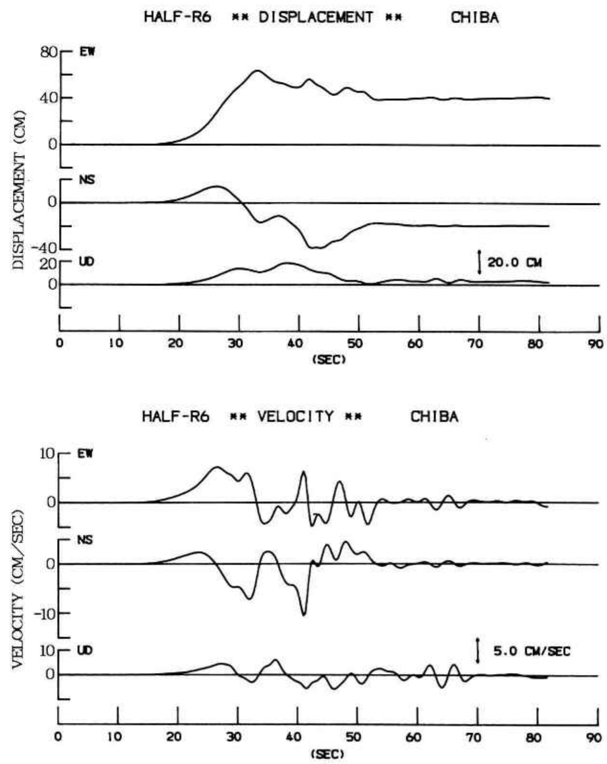

Fig. 12b Synthesized displacement (upper) and velocity (lower) waveforms at Chiba for the half-space model. The unit of vertical axis is shown in the figure.

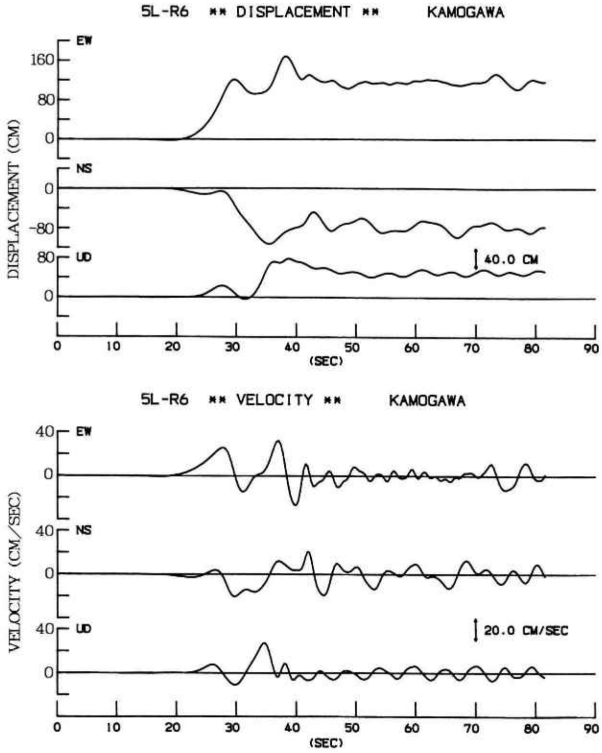

Fig. 13a Synthesized displacement (upper) and velocity (lower) waveforms at Kamogawa for the layered structure model. The unit of vertical axis is shown in the figure.

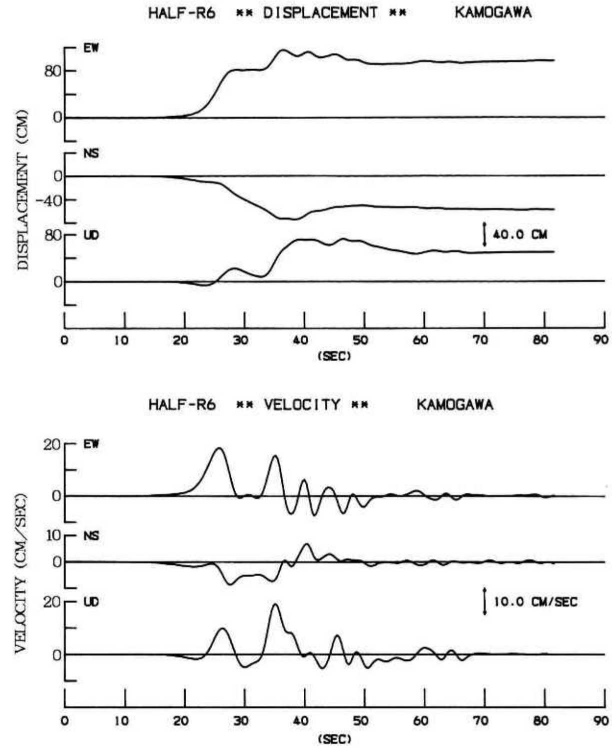

Fig. 13b Synthesized displacement (upper) and velocity (lower) waveforms at Kamogawa for the half-space model. The unit of vertical axis is shown in the figure.

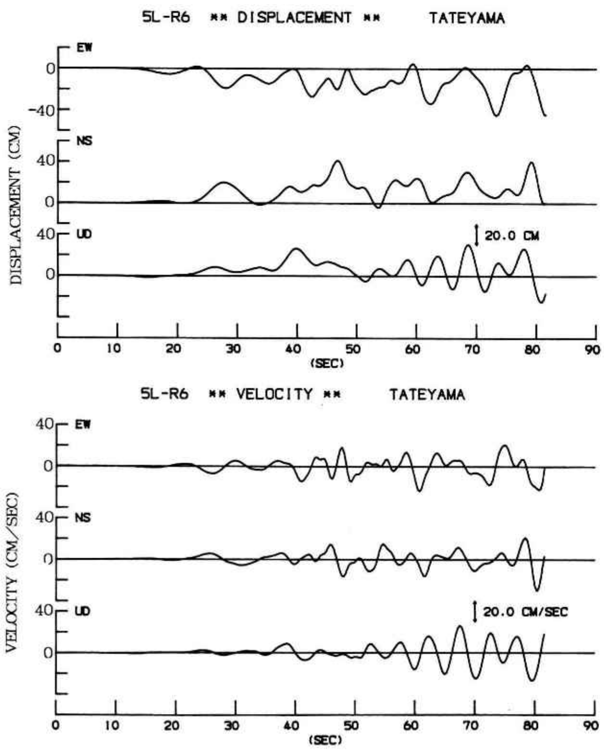

Fig. 14a Synthesized displacement (upper) and velocity (lower) waveforms at Tateyama for the layered structure model. The unit of vertical axis is shown in the figure.

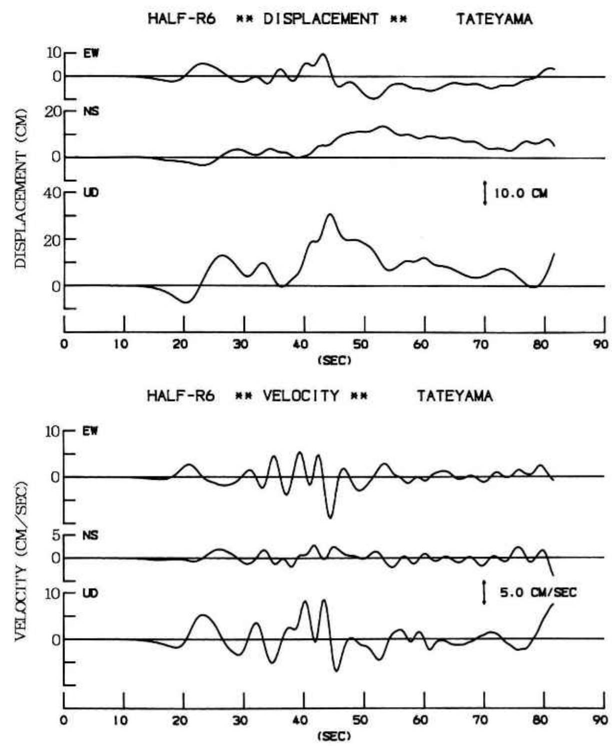

Fig. 14b Synthesized displacement (upper) and velocity (lower) waveforms at Tateyama for the half-space model. The unit of vertical axis is shown in the figure.

displacements at Kamogawa for the half-space model (Fig. 13b) show a steplike change similar to Hatano, and the amplitude at Kamogawa is comparable to or slightly smaller than Hatano (compare Fig. 10b and Fig. 13b). However, the monotonical wavetrain is not as developed in this case as at Hatano.

The last site, Tateyama, a city on the southern tip of the Boso Peninsula, is the nearest of the seven sites to the fault edge, and the distance from the epicenter is about 60km. The synthetic waveforms at Tateyama are shown in Fig. 14a and Fig. 14b. The nature of the displacement waveform is quite different from all of the previous cases, probably because Tateyama is located on the foot-wall side of the fault. Although the static deformation is as small as about 20cm or less for both the EW and NS components, the displacement waveform seems the most complex among the seven sites, even for the half-space synthetics (Fig. 14a and Fig. 14b). In the velocity waveform, rather short period waves of 2-4 seconds are predominant, and the amplitudes of those waves are comparable to those at Fuchu.

5. Response Spectra of the Synthesized Ground Motions

To evaluate the effect of ground motion upon large-scale structures, we compute the response spectrum by using the synthesized waveforms of the previous section for input ground motions. The response spectrum is a simple but important measure in engineering seismology, which represents a maximum response motion of a simple mass-spring vibration system as a function of the eigen-period and damping factor of the vibration system. By illustrating the response spectrum, we can get an insight into not only the characteristic nature of the ground motion itself but also the influences upon the structure.

The velocity response spectra, $F_v(T,h)$, for horizontal motions at Tokyo and the other sites are shown in Figs. 15 through 21. Since the response spectra are plotted in the tripartite coordinate system, the acceleration and displacement responses are immediately read from the figures. In those figures, the left figure represents the response spectrum of the EW component and the right, the NS component. The three response curves in each figure correspond to the damping of h=0.01, 0.05, and 0.1, respectively. The letters a and b added to the figure number represent the response spectrum of the synthesized waveform computed for the layered medium and for the half-space model, respectively. At Tokyo, for instance, the response of a structure that has a fundamental period of 10-13 seconds and a damping of h=0.01 is read as large as 200cm in displacement, 100cm/sec in velocity, and 50cm/sec^2 in acceleration in the case of the layered model (Fig. 15a).

The acceleration response spectrum, $F_a(T,h)$, is directly related to the base shear coefficient, C_b. The base shear coefficient, playing an important role in aseismic designing, is represented by the ratio of the maximum shearing force acting on a structure during an earthquake to the total weight of the structure; $C_b = M \cdot F/M \cdot g$, where M is the total mass and g is the acceleration of gravity. According to the 1973 draft called "Guidelines for Aseismic Design of Tall Buildings" by the Architectural Institutes of Japan (AIJ), the design base shear coefficient is recommended to be $C_b=(0.15 \sim 0.3)/T$ for T longer than 1 second, where T is the fundamental period of a structure. Simply speaking, if a structure encounters a large acceleration for which the base shear far exceeds the AIJ recommendation, the structure may be placed in a difficult situation.

The AIJ recommendation for the design base shear coefficient is shown by the shaded zone in each of the figures from Fig. 15 to Fig. 21. The recommended zone in terms of velocity response does not depend on T because $F_a = g \cdot C_b$, and $F_v = (T/2\pi) \cdot F_a$, then $F_v = (0.15 \sim 0.3)(g/2\pi)$. The most severe case is seen in the response spectrum at Hatano shown in the left side of Fig. 17a. At this site, the response curves have two conspicuous peaks at 4-5 seconds and about 7 seconds. The displacement responses at those peaks are as large 200cm and over 300cm, respectively, and the velocities of 250-300cm/sec at both peaks show five or six times larger values than the AIJ recommendation. Moreover, the acceleration at those peaks reach about 250-300cm/sec^2. Such large accelerations in that period range may not have been observed or recorded in actual earthquakes since the beginning of modern engineering seismology. The responses for the half-space model fall almost within the range of the recommendation.

6. Discussion and Conclusion

Strong ground motions excited by a major earthquake like the Kanto Earthquake of 1923 were theoretically predicted for seven sites in and around the Toyko metropolitan area. To simulate realistic ground motions, we adopted the layered underground structure with thick sedimentary layers (Fig. 1) and the complex faulting process (Figs. 3, 4, 5). The pres-

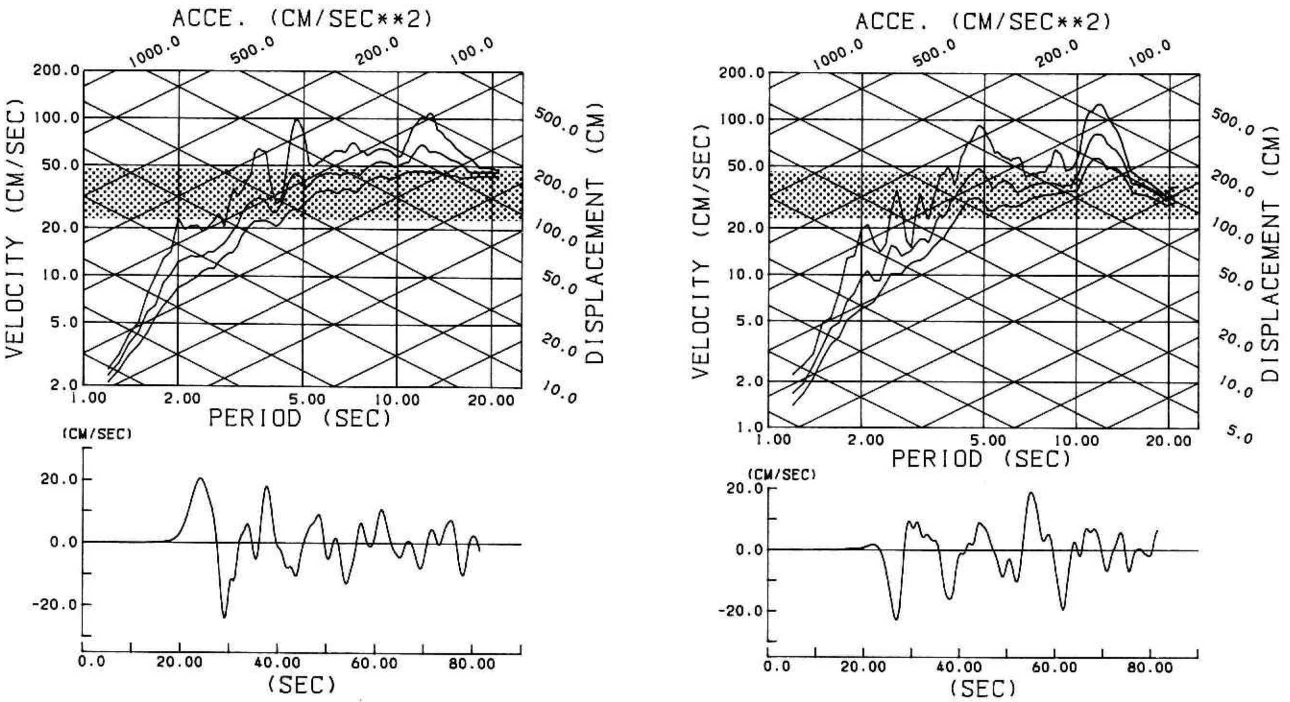

Fig. 15a Tripartite representation of the response spectra of the synthetic EW (left) and NS (right) ground motion at Tokyo for the layered structure model. The three curves correspond to damping factors of 0.01, 0.05, and 0.1.

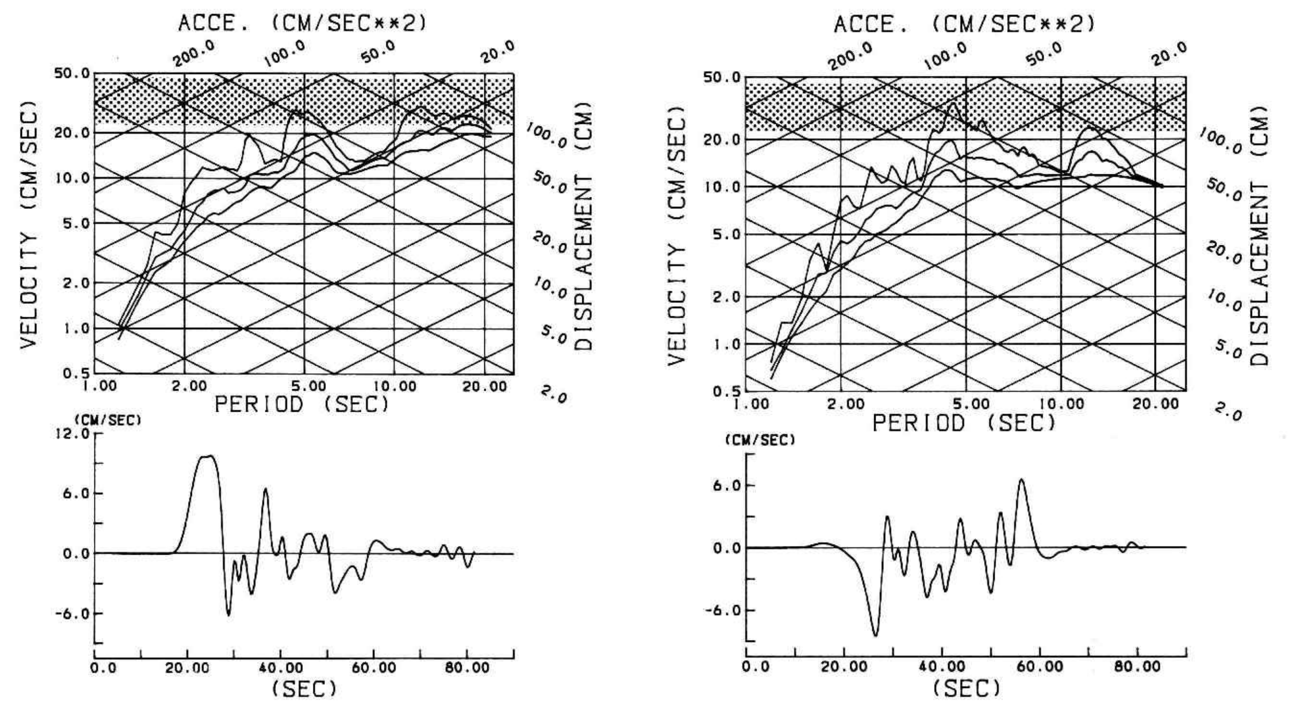

Fig. 15b Tripartite representation of the response spectra of the synthetic EW (left) and NS (right) ground motion at Tokyo for the half-space model. The three curves correspond to damping factors of 0.01, 0.05, and 0.1.

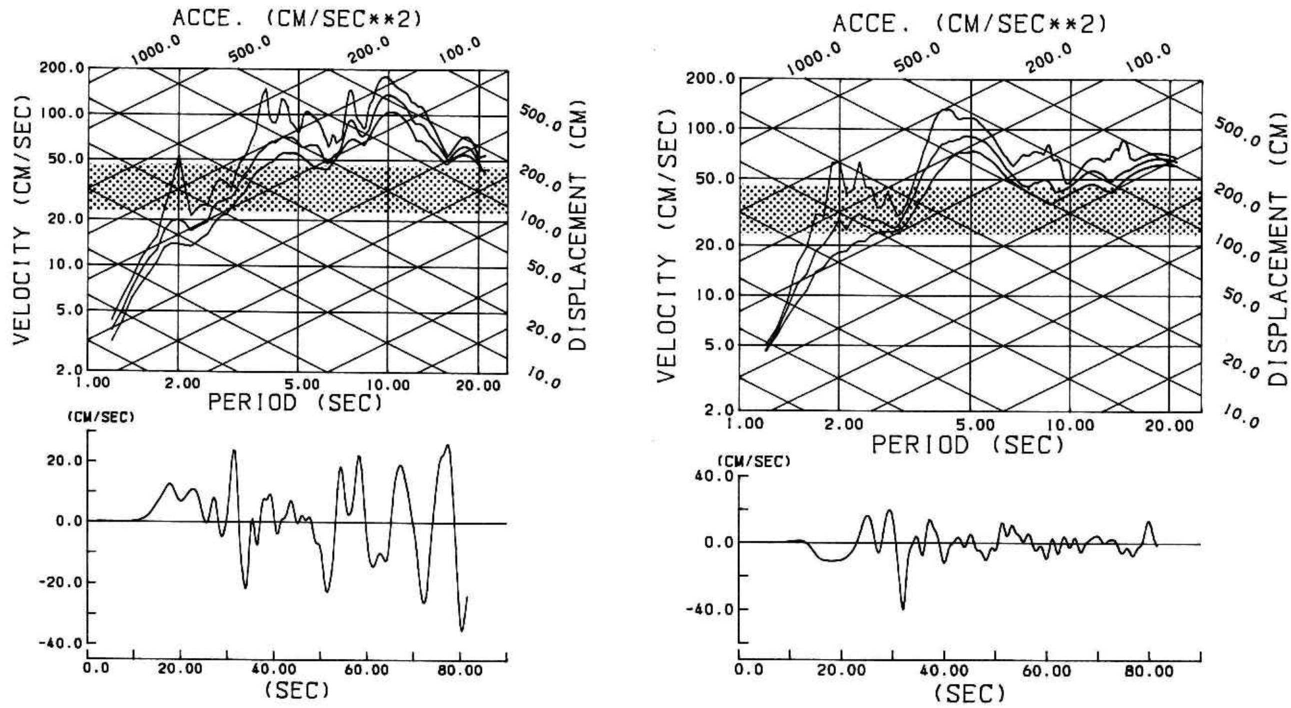

Fig. 16a Tripartite representation of the response spectra of the synthetic EW (left) and NS (right) ground motion at Yokohama for the layered structure model. The three curves correspond to damping factors of 0.01, 0.05, and 0.1.

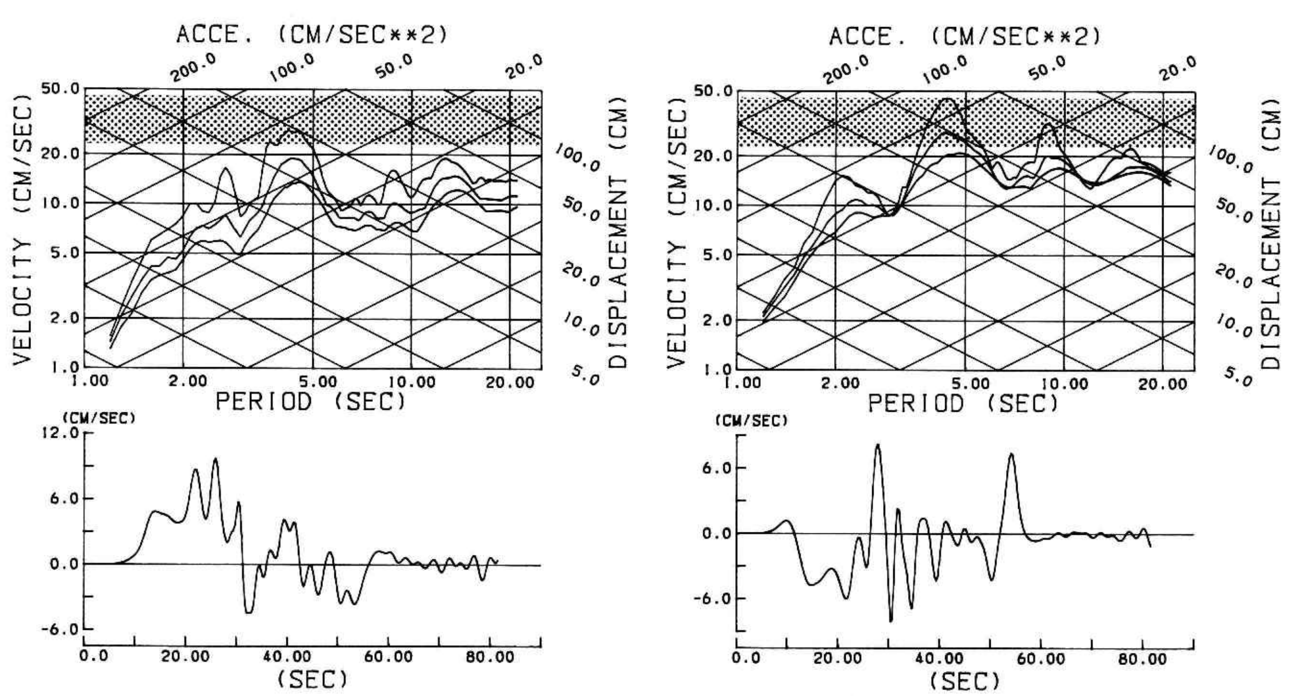

Fig. 16b Tripartite representation of the response spectra of the synthetic EW (left) and NS (right) ground motion at Yokohama for the half-space model. The three curves correspond to damping factors of 0.01, 0.05, and 0.1.

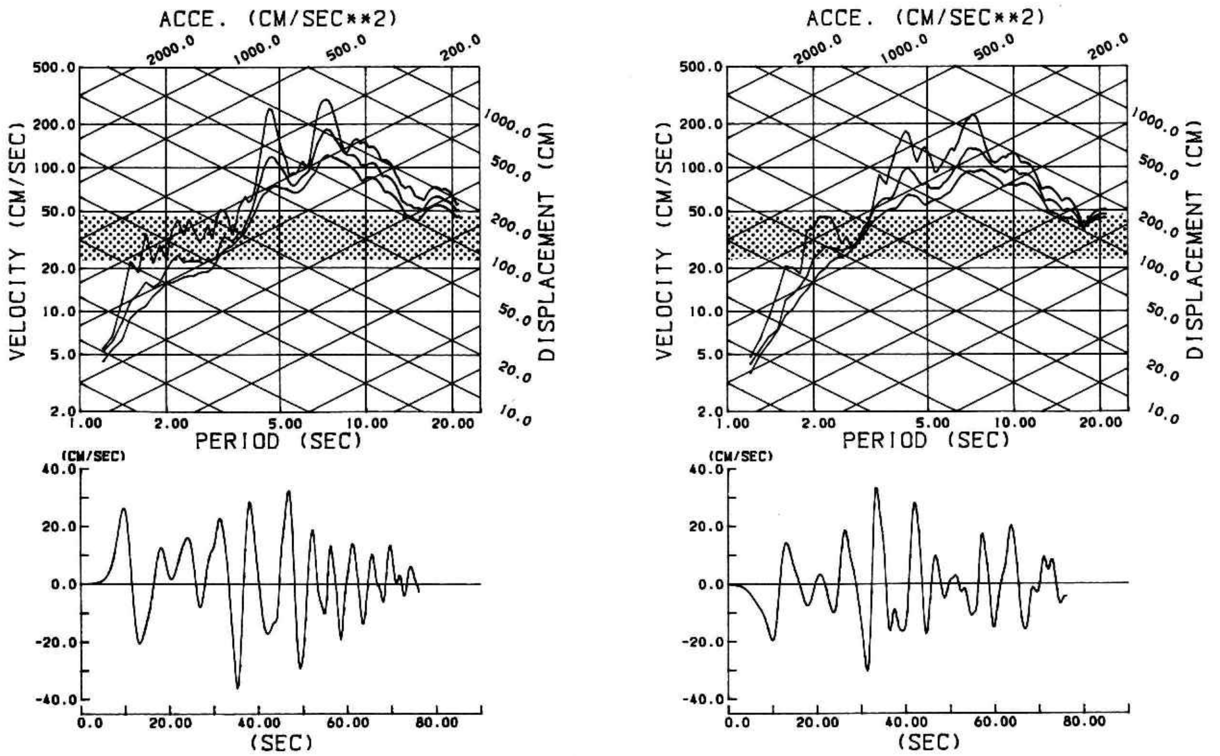

Fig. 17a Tripartite representation of the response spectra of the synthetic EW (left) and NS (right) ground motion at Hatano for the layered structure model. The three curves correspond to damping factors of 0.01, 0.05, and 0.1.

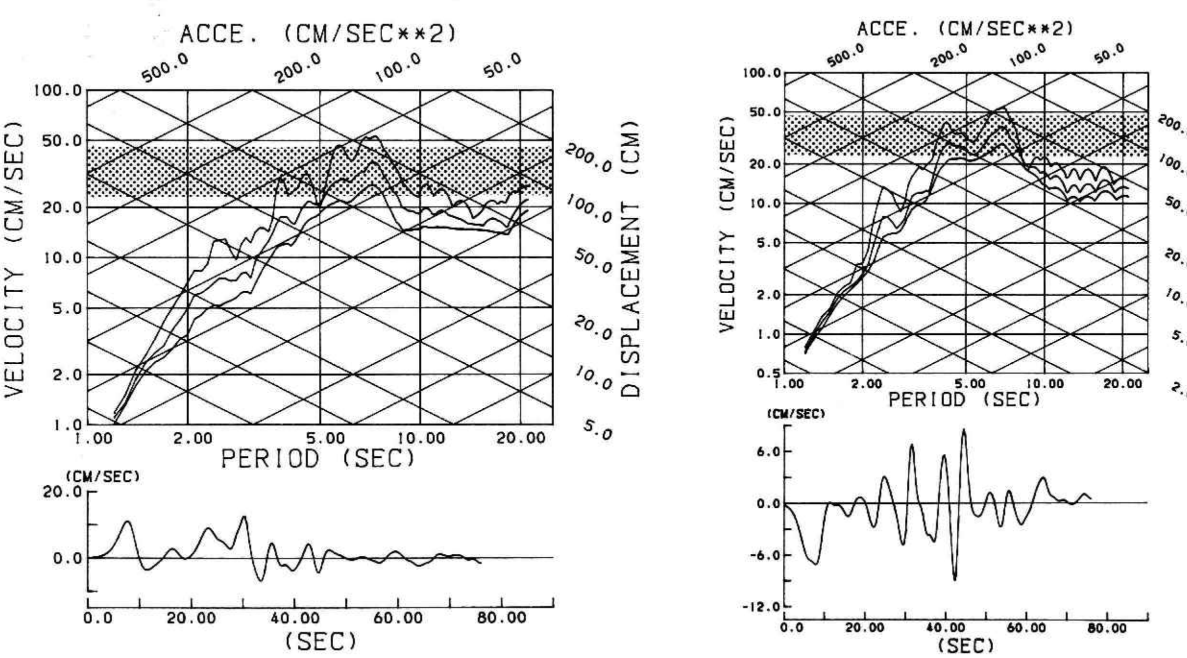

Fig. 17b Tripartite representation of the response spectra of the synthetic EW (left) and NS (right) ground motion at Hatano for the half-space model. The three curves correspond to damping factors of 0.01, 0.05, and 0.1.

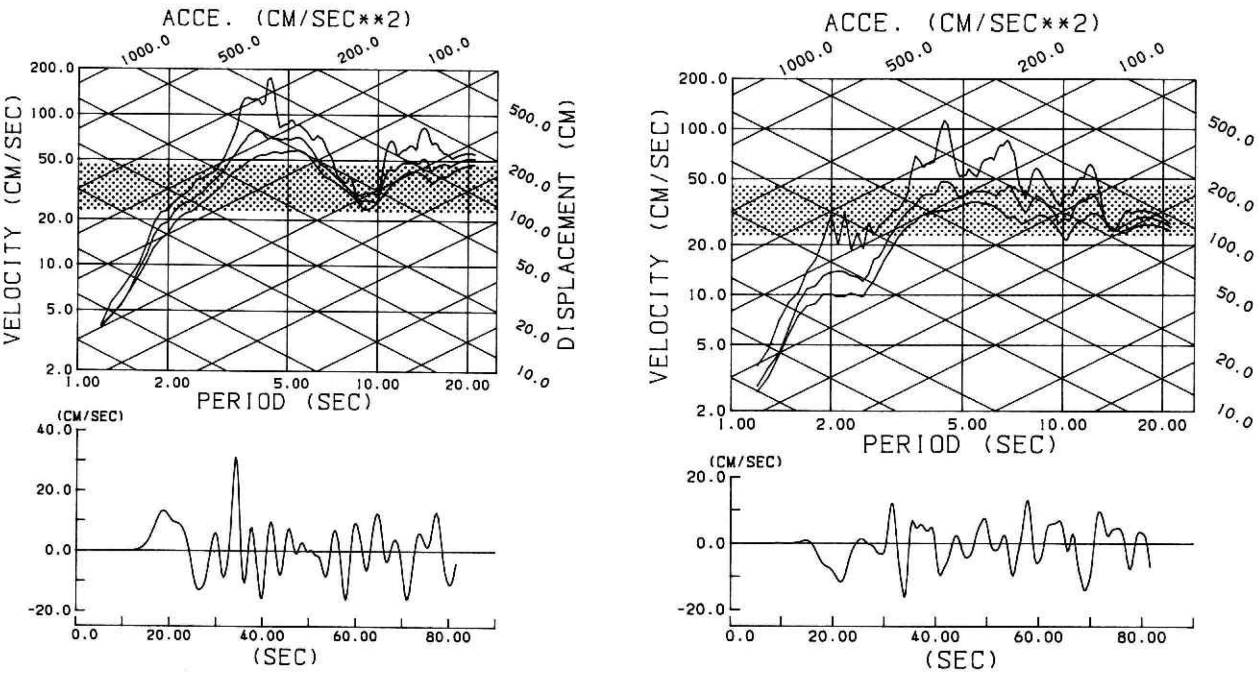

Fig. 18a Tripartite representation of the response spectra of the synthetic EW (left) and NS (right) ground motion at Fuchu for the layered structure model. The three curves correspond to damping factors of 0.01, 0.05, and 0.1.

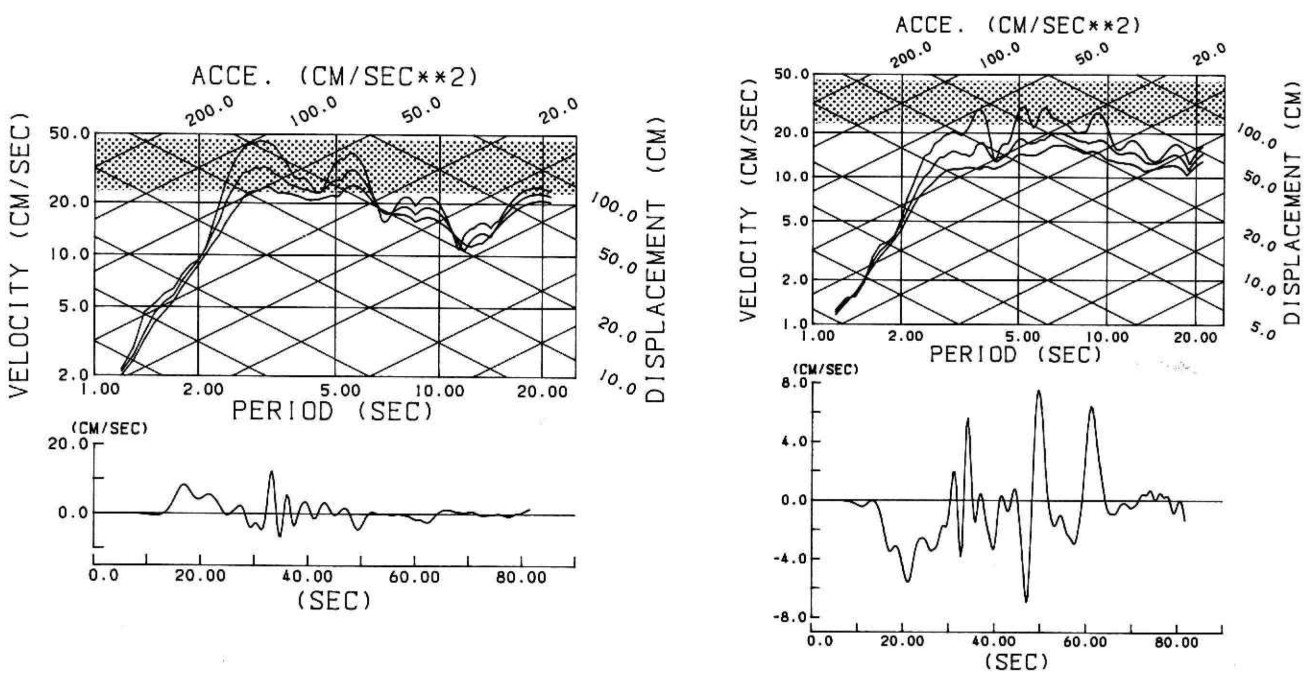

Fig. 18b Tripartite representation of the response spectra of the synthetic EW (left) and NS (right) ground motion at Fuchu for the half-space model. The three curves correspond to damping factors of 0.01, 0.05, and 0.1.

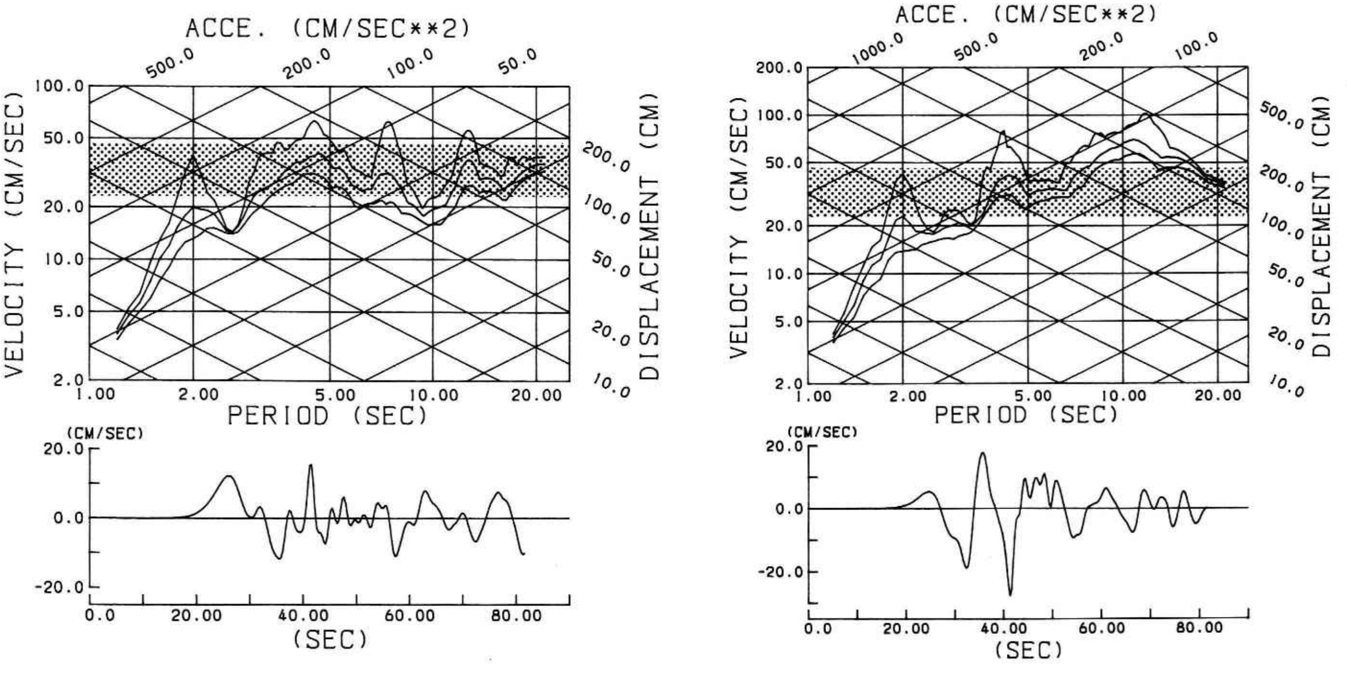

Fig. 19a Tripartite representation of the response spectra of the synthetic EW (left) and NS (right) ground motion at Chiba for the layered structure model. The three curves correspond to damping factors of 0.01, 0.05, and 0.1.

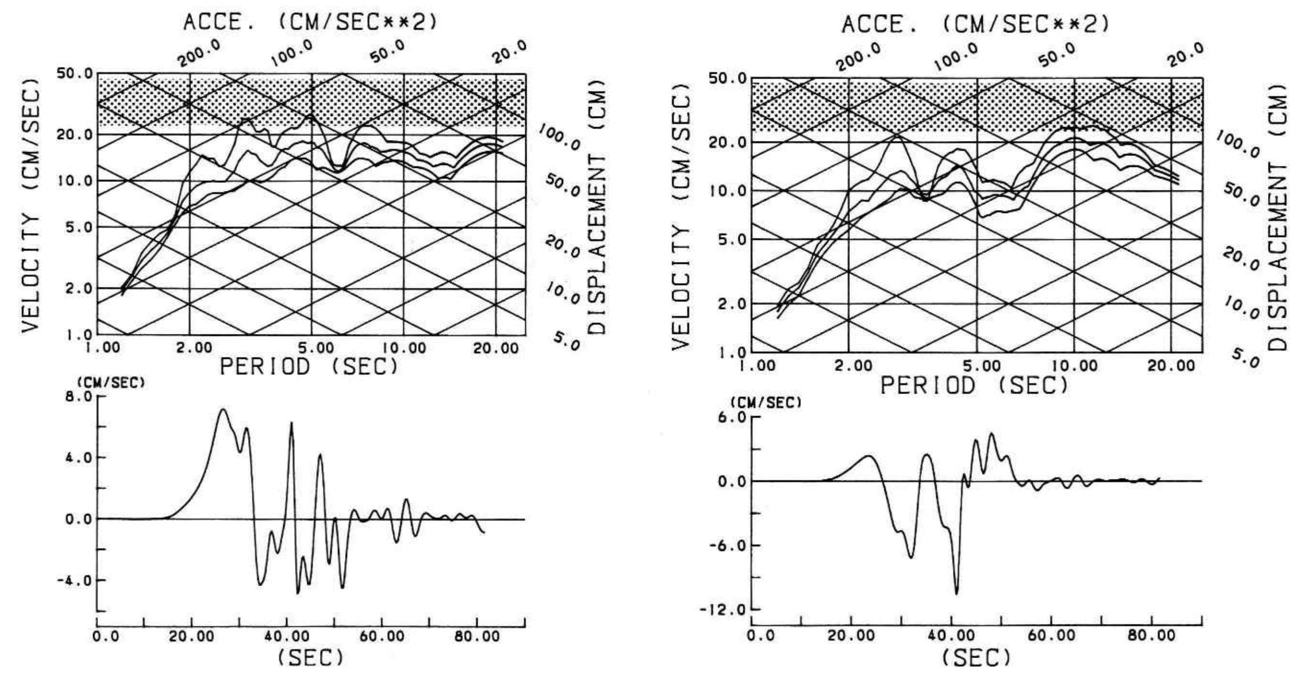

Fig. 19b Tripartite representation of the response spectra of the synthetic EW (left) and NS (right) ground motion at Chiba for the half-space model. The three curves correspond to damping factors of 0.01, 0.05, and 0.1.

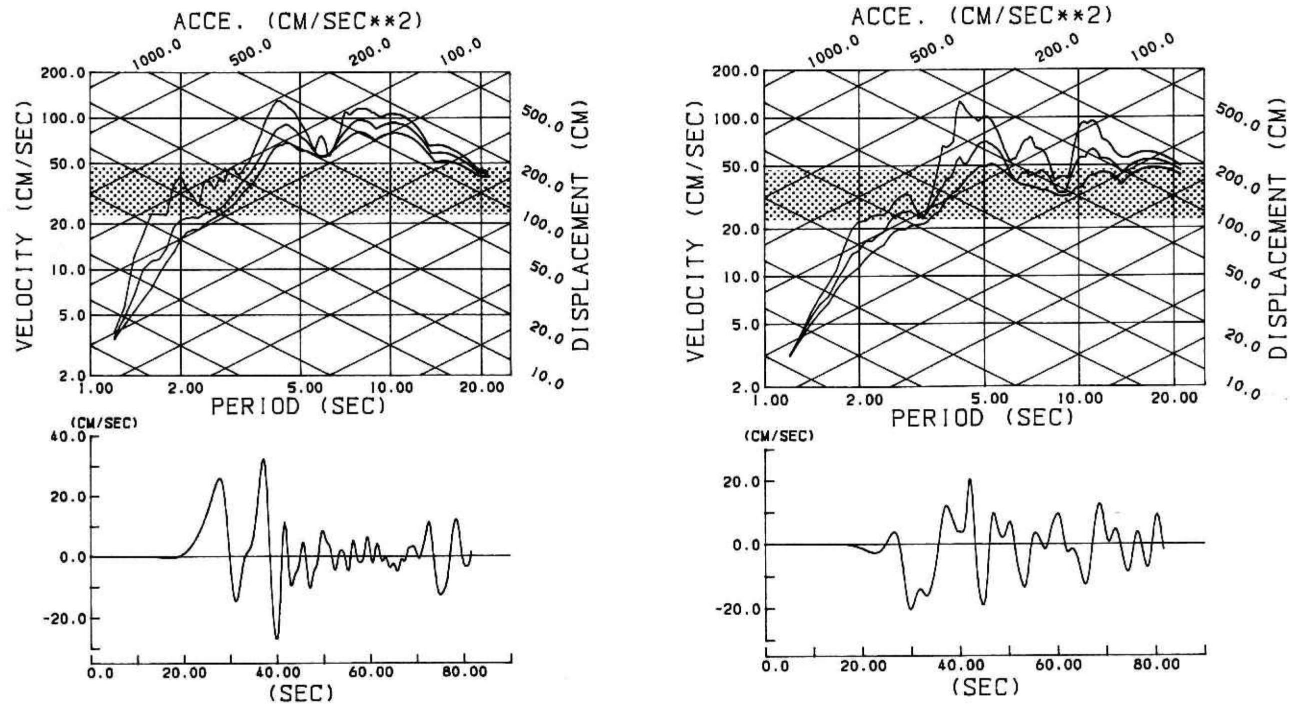

Fig. 20a Tripartite representation of the response spectra of the synthetic EW (left) and NS (right) ground motion at Kamogawa for the layered structure model. The three curves correspond to damping factors of 0.01, 0.05, and 0.1.

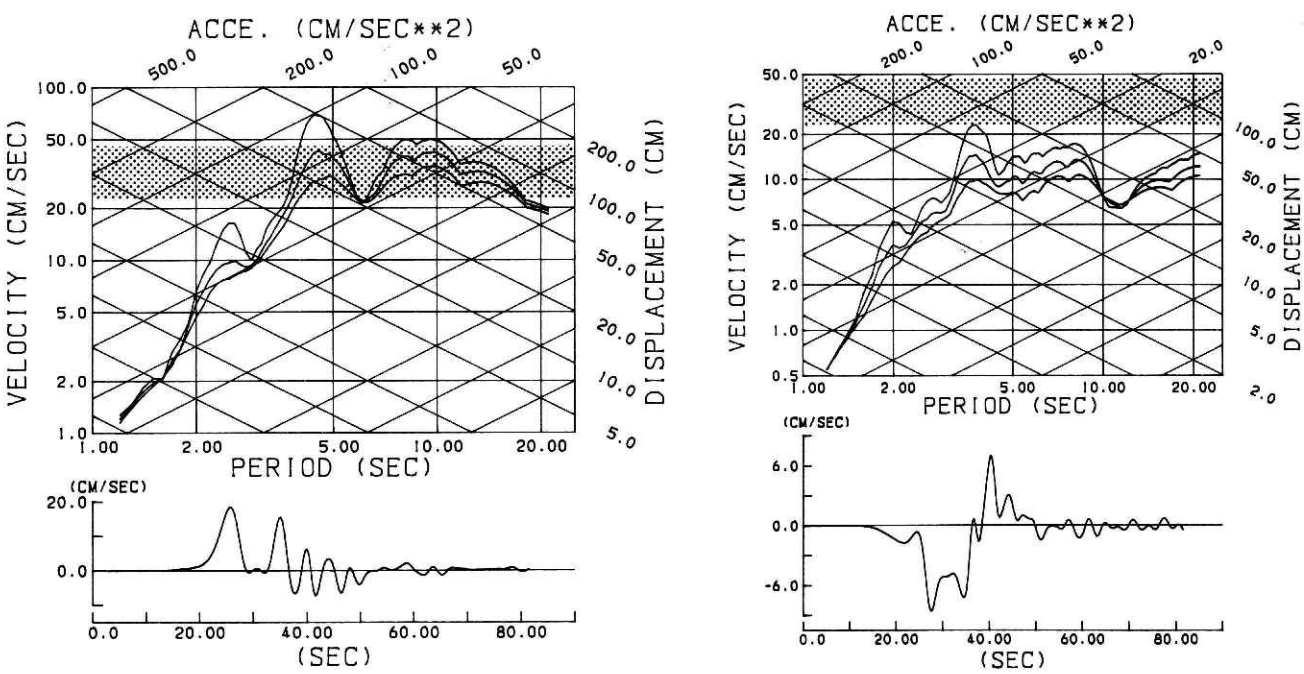

Fig. 20b Tripartite representation of the response spectra of the synthetic EW (left) and NS (right) ground motion at Kamogawa for the half-space model. The three curves correspond to damping factors of 0.01, 0.05, and 0.1.

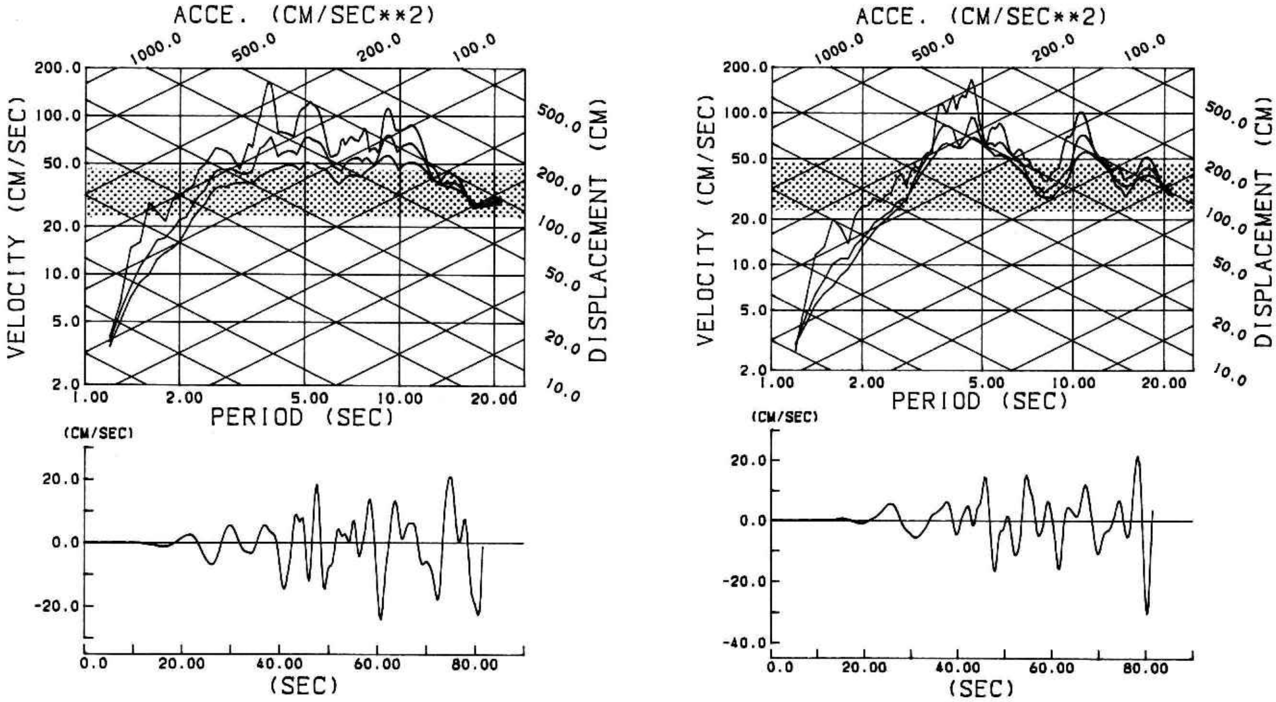

Fig. 21a Tripartite representation of the response spectra of the synthetic EW (left) and NS (right) ground motion at Tateyama for the layered structure model. The three curves correspond to damping factors of 0.01, 0.05, and 0.1.

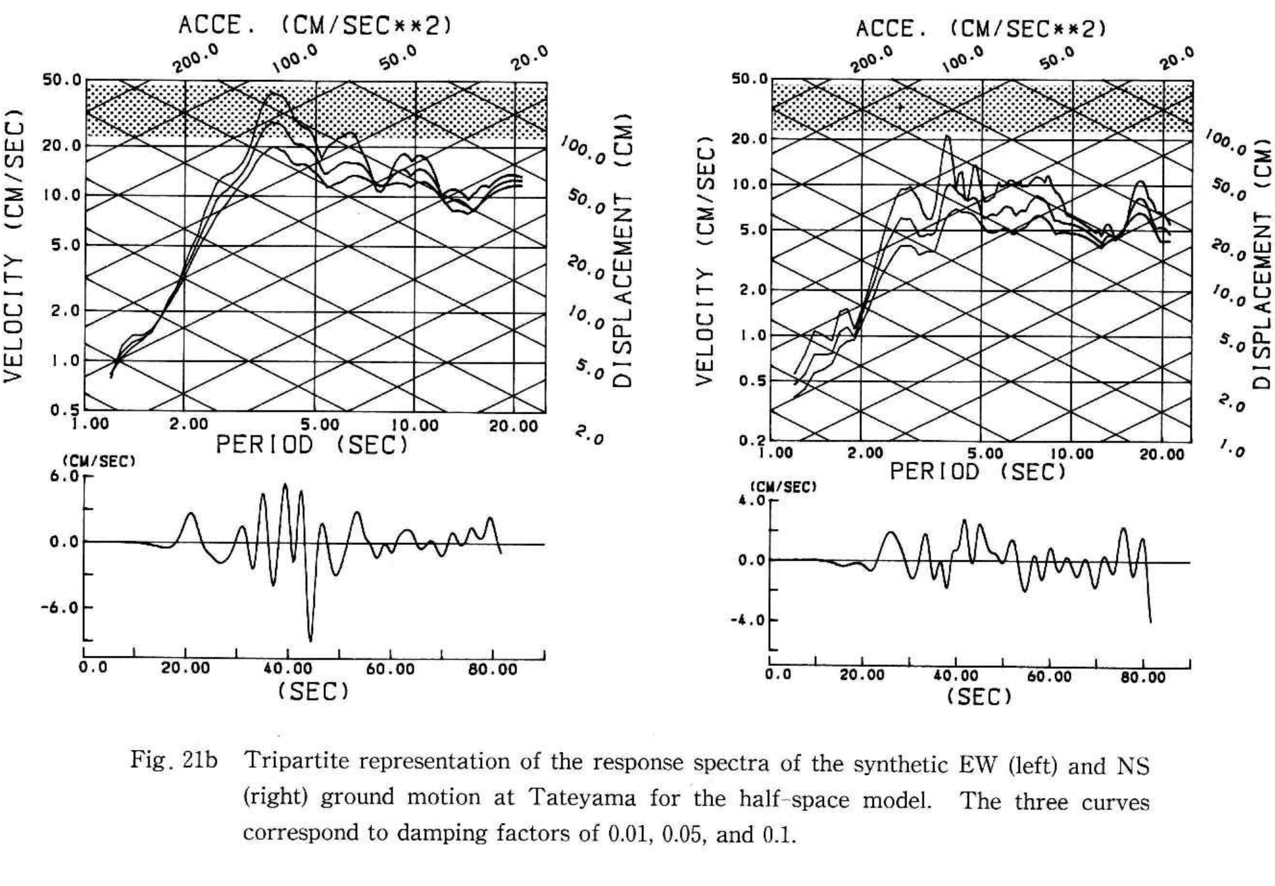

Fig. 21b Tripartite representation of the response spectra of the synthetic EW (left) and NS (right) ground motion at Tateyama for the half-space model. The three curves correspond to damping factors of 0.01, 0.05, and 0.1.

ent simulation showed that the ground motions synthesized for the realistic layered medium have very complex and amplified features in comparison with those for the half-space model. The complex motions excited by the inhomogeneous rupture process are considerably modulated into more and more complicated forms through the effect of the sedimentary layers (see Figs. 8-14).

The synthesizing technique can also be applied to the shorter period waves of less than 1 second. To change the rupture process into a more complicated one is easily accomplished by dividing the fault surace into sufficiently smaller sub-faults. But, the finer the sub-fault division, the larger the computation becomes. However, such time-consuming work will not bring about fruitful results beause we lack detailed information on the local site conditions including the soft alluvial layers.

From an engineering point of view, we evaluated synthesized ground motion in terms of the response spectra. The response spectra estimated suggest that the structures in and around the Tokyo metropolitan area which have a fundamental period longer than about 3 seconds may be put into a much severer situation when a large earthquake occurs than was previously expected. The example at Tokyo indicates that the maximum response of a structure having a fundamental period of 10-13 seconds is as large as 200cm in displacement, 100cm/sec in velocity, and 50cm/sec^2 in acceleration. The velocity, 100cm/sec, gives a base shear twice as large as the upper limit of the AIJ recommendation, $C_b=(0.15\sim0.3)/T$. According to Ohtani (1977), most of the actual high-rise buildings are designed to meet more a severe criterion than the AIJ recommendation, $C_b=(0.24\sim0.42)/T$. The acceptance of this severe criterion tells us that designers endow a sufficient capacity on structures in order to secure safety, even if it causes the cost to be a little higher. It should be noted that high-rise buildings have never experienced a destructive earthquake, and their safety has not yet been put to the test in practice.

Acknowledgements

The author wishes to express his sincere thanks to Prof. M. Ohtake of Tohoku University for his continuous support and suggestions, and critical reading of this manuscript. I am greatly indebted to Mrs. Y. Nakagawa for her assistance in drawing the figures.

References

1) Aki, K. (1968) : Seismic displacement near a fault, J. Geophys. Res., **73**, 5359-5376.
2) Aki, K. (1982) : Strong motion prediction using mathematical modeling techniques, Bull. Seismol. Soc. Am., **72** Special Issue, S29-S41.
3) Aki, K. and P. G. Richards (1980) : Quantitative Seismology : Theory and Methods, Volume I, W. H. Freeman and Company, San Fransisco, California, pp 557.
4) Aspel, R. J. (1979) : Dynamic Green's functions for layered media and applications to boundary-value problems, Ph. D. thesis, Univ. Calif., San Diego, La Jolla, California.
5) Aspel, R. J. and J. E. Luco (1983) : On the Green's functions for a layered halfspace, Part II, Bull. Seismol. Soc. Am., **73**, 931-951.
6) Bouchon, M. (1979a) : Discrete wavenumber representation of elastic wave fields in three space dimensions, J. Geophys. Res., **84**, 3609-3614.
7) Bouchon, M. (1979b) : Predictability of ground displacement and velocity near earthquake fault. An example : The Parkfield earthquake of 1966, J. Geophys. res., **84**, 6149-6156.
8) Bouchon, M. (1981) : A simple method to calculate Green's functions for elastic layered media, Bull. Seismol. Soc. Am., **71**, 959-971.
9) Bouchon, M. and K. Aki (1977) : Discrete wavenumber representation of seismic-source wave field, Bull. Seismol. Soc. Am., **67**, 259-277.
10) Fucks, K. (1968) : The reflection of spherical waves from transition zones with arbitrary depth-depesdent elastic moduli and density, J. Phys. Earth, **16**, Suppl., 27-41.
11) Fucks, K. and G. Muller (1971) : Computation of synthetic seismograms with the reflectivity method and comparison with observations, Geophys. J. R. astro. Soc., **23**, 417-433.
12) Heaton, T. H. and D. V. Helmberger (1977) : A study of the strong ground motion of the Borrego Mountain, California, earthquake, Bull. Seismol. Soc. Am., **67**, 315-330.
13) Heaton, T. H. and D. V. Helmberger (1978) : Predictability of strong ground motion in the Imperial valley : modeling the M4.9 November 4, 1976 Brawley earthquake, Bull. Seismol. Soc. Am., **68**, 31-48.
14) Helmberger, D. V. (1974) : Generalized ray theory for shear dislocations, Bull. Seimol. Soc. Am., **64**, 45-64.
15) Helmberger, D. V. and D. A. Harkrider (1978) :

Modeling earthquakes with generalized ray thetry, in J. Miklowitz and J. D. Achenbach (editors), Medern Problems in Elastic Wave Proragation, New York, Wiley.
16) Kanamori, H. (1972): Determination of effective tectonic stress associated with erthquake faulting. The Tottori Earthquake of 1943, Phys Earth Planet. Interior, **5**, 426-434.
17) Kanamori, H. (1974): Long-period ground motion in the epicentral area of major earthquakes, Tectonophys., **21**, 341-356.
18) Kawasaki, I., Y. Suzuki, and R. Sato (1973): Seismic wave due to a shear fault in a semi-infinite medium. Part I: Point source, J. Phys. Earth, **21**, 251-284.
19) Kawasaki, I., Y. Sukuki, and R. Sato (1975): Seismic wave due to a shear fault in a semi-infinite medium. Part II: Moving soure, J. Phys. Earth, **23**, 43-61.
20) Kennett, B. L. N. (1980): Seismic waves in a stratified half space - II. Theoretical seismograms, J. R. astr. Soc., **61**, 1-10.
21) Kennett, B. L. N. and N. J. Kerry (1979): Seismic waves in a stratified half space, Geophys. J. R. astr. Soc., **57**, 557-583.
22) Kohketsu, K. (1985): The extended reflectivity method for synthetic near-field seismograms, J. Phys. Earth, **33**, 121-131.
23) Kudo, K. (1978): Surface waves as input motions to a large scale structure, Proceedings of the 5th Japan Earthquake Engineering Symposium, 273-280 (in Japanese).
24) Luco, J. E. and R. J. Aspel (1983): On the Green's function for a layered half-space. Part I, Bull. Seismol. Soc. Am., **73**, 909-929.
25) Miyatake, T. (1980a): Numerical simulation of earthquake source process by a three-dimensional crack model. Part 1. Rupture process, J, Phys. Earth, **28**, 565-598.
26) Miyatake, T. (1980b): Numerical simulation of earthquake source process by a three-dimensional crack model. Part 2. Seismic waves and spectrum, J. Phys. Earth, **28**, 599-616.
27) Ohta, Y. and H. Kagami (1976): Ultimate values of period and amplitude on seismic input motions in relation to a large-scale structure, Trans. Archit. Inst. Japan, **249**, 53-59 (in Japanese).
28) Ohta, Y., N. Goto, K. Shiono, H. Takahashi, F. Yamamizu, and S. Kurihara (1977): Shear wave velocities in deep soil deposits - Measurement in a borehole to the depth of 3500 meters and its significance, Zishin (J. Seismol. Soc. Japan), Ser. 2, **30**, 415-433 (in Japanese).
29) Ohta, Y., N. Goto, K. Shiono,H. Takahashi, F. Yamamizu, and S. Kurihara (1978): Shear wave velocities in deep soil deposits. Part II - Measurement in a borehole of Shimofusa observatory to the depth of 2300 meters, Zishin (J. Seismol. Soc. Japan), Ser. 2, **31**, 299-308 (in Japanese).
30) Ohta, Y., N. Goto, F. Yamamizu, and H. Takahashi (1980): S wave velocity measurements in deep soil deposit and bedrock by means of an elaborated down-hole method, Bull. Seismol. Soc. Am., **70**, 363-377.
31) Ohtani, K. (1977): Earthquake resistant design of high-rise buildings in Japan, Proceedings of the 9th Joint UJNR Panel Conference, Wind and Seismic Effects, NBS Special Publication, No. 523, VI, 15-24.
32) Seo, K. (1979): Propagation of body waves in the southern Kanto region derived from observed initial motions of earthquakes, Zishis (J. Seismol. Soc. Japan), Ser 2, **32**, 267-280 (in Japanese).
33) Seo, K. and H. Kobayashi (1980): On the seismic prospectings in the southwestern part of the Tokyo Metropolitan Area - Underground structure along the line stations from Yumenoshima, Tokyo to Enoshima, Kanagawa -, Zishin (J. Seismol. Soc. Japan), Ser. 2, **33**, 23-36 (in Japanese).
34) Shima, E., M. Yanagisawa, K. Kudo, T. Yoshii, Y. Ichinose, K. Seo, K. Yamazaki, N. Ohbo, Y. Yamamoto, Y. Oguchi, and M. Nagano (1976a): On the base rock of Tokyo. Observations of seismic waves generarated from the 1st and 2nd Yumenoshima explosions, Bull. Earthq. Res. Inst., Univ. Tokyo, **51**, 1-11 (in Japanese).
35) Shima, E., M. Yanagisawa, K. Kudo, K. seo, and K. Yamazaki (1976b): On the base rock of Tokyo. II: Observations of seismic waves generated from the 3rd Yumenoshima and Yoshikawa explosions, Bull. Earthq. Res. Inst., Univ. Tokyo, **51**, 45-61 (in Japanese).
36) Suzuki, H., R. Ikeda, T. Mikoshiba, S. Kinoshita, H. Sato, and H. Takahashi (1981): Deep well logs in the Kanto-Tokai area, Rev. Res. Disaster Prevention, **65**, 1-162 (in Japanese).
37) Takahashi, H. (1982): The deep-borehole observatories and their contribution for revealing the characteristics of microearthquake activity in the Kanto district, Rep. Nat. Res. Center. Disaster Prevention, **28**, 1-104 (in Japanese).
38) Takeo, M. (1985): Near-field synthetic seismograms taking into account the effects of anelasticity - The effects of anelastic attenuation on

seismograms caused by a sedimentary layer, Papers Meteorol. Geophys., **36**, 245-257 (in Japanese).

39) Yamamizu, F. and N. Goto (1978) : Direct measurement of seismic wave velocities in deep soil deposits, Proceedings of the 5th Japan Earthquake Engineering Symposium, 329-336.

40) Yamamizu, F., H. Takahashi, N. Goto, and Y. Ohta (1981) : Shear wave velocities in deep soil deposits. Part III - Measurements in the borehole of the Fuchu observatory to the depth of 2750m and a summary of the results -, Zishin (J. Seismol. Soc. Japan). Ser. 2, **34**, 465-479 (in Japanese).

41) Yamamizu, F., N. Goto, H. Takahashi, Y. Ohta (1983) : Attenuation of shear waves in deep soil deposits as revealed by down-hole measurements in the 2,300meter borehole of the Shimohsa Observatory, Japan, J. Phys. Earth, **31**, 139-157.

42) Yao, Z. X. and D. G. Harkrider (1983) : A generalized reflection-transmission coefficient matrix and discrete wavenumber method for synthetic seismograms, Bull, Seismol. Soc. Am., **73**, 1685-1699.

(Accepted : 22 July 1996)

厚い堆積層の影響を考慮した震源近傍における強震動のシミュレーション

山水史生*

防災科学技術研究所

要旨

1923年関東地震のような大地震を想定して，震源域における強震動の理論的合成を，首都圏近郊の7地点(東京・横浜・泰野・府中・千葉・鴨川・館山）において行った．その合成には，不均質断層破壊過程と厚い堆積層の影響を考慮した．これらの合成地震動は，半無限媒質における結果と比較して，厚い堆積層の影響が極めて大きいことを明瞭に示している．地震工学的見地から，合成された地震動の建築物への影響を評価するため応答スペクトルを計算した．応答スペクトルは、やや長周期領域に基本モードを持つ建築物への顕著な影響を示唆している。3秒以上の長周期領域においては，上記7地点全てにおいて，ベースシア係数がAIJ(日本建築学会)基準の上限値を越えることが示された。

Key words : Strong Ground Motion（強震動）, Near Field（近地地震）,
Inhomogeneous Source（不均質震源）, Deep Soil Deposits（厚い堆積層）,
Simulation（シミュレーション）, Kanto Earthquake（関東地震）